2017

Uncertainty Analysis of a Multifunctional Tribometer

Michael Andrew Goldstein
Lehigh University

Uncertainty Analysis of a Multifunctional Tribometer

By

Michael A Goldstein

A Thesis

Presented to the Graduate and Research Committee

Of Lehigh University

In Candidacy for the Degree of

Master of Science

In

Mechanical Engineering

Lehigh University

January 2017

This thesis is accepted and approved in partial fulfillment of the requirements for the Master of Science.

_____

Date

_____

Dr. Brandon Krick, Thesis Advisor

_____

Dr. D. Gary Harlow, Chairperson of Department

Acknowledgements

I would like to acknowledge the help of everyone in the Lehigh Tribology Laboratory, especially Dr. Brandon Krick for taking me on for this project along with John Curry for building the tribometer that all of this work was based on. Additional thanks goes to the WD40 Corporation and Michael Counts for providing the funding for this project. Finally, I'd like to thank my parents, Jeff and Lorraine for their unwavering love, help, and support; I couldn't be where I am today without them.

Table of Contents

List of Tables

List of Figures

Abstract

In response to the high cost and limited instrumentation available on commercial tribometers a student designed tribometer was conceived, built, and tested. This tribometer combines multiple tribology testing configurations into a single compact and reconfiguration tribometer, dubbed the multifunctional tribometer. This tribometer is also capable of operating in expanded experimental spaces not covered within the limited scope of industry standardized tribological tests. Specifically, this tribometer is able to conduct rotary tests in a reciprocating fashion; this capability is unavailable on any other tribometer published so far in literature or available commercially.

Following an overview of the industry standards and the tribometer's capability is an uncertainty analysis for the reciprocating block on ring testing regime of the multifunctional tribometer. As this test method is totally unique to this machine it is necessary to prove its validity and accuracy. This is done through the use of an uncertainty analysis which is then expanded across all experimental spaces covered by the testing configuration. Additionally, an uncertainty budget has been made which shows what aspects of the machine would be most worthwhile to upgrade to improve performance.

Finally, a case study is included which involves an experiment testing the lubrication properties of WD40 in this reciprocating block on ring configuration of the multifunctional tribometer.

Background

Tribology is the study of friction and wear along with their effects. These effects have huge implications, studies have predicted that improvements in tribology can save countries money on the order of 1% of their GDP per year, thus the impetus for researching these phenomena are clear.[1,2] Typical tribological experiments seek to define the wear rate and friction coefficient of different material systems through physical testing. These tests take many different forms. Wear is highly variable and dependent not only on the materials involved, but also their geometries, surface finishes, the presence of lubrication, and the local environment.[3] The ASTM maintains many standards of different types of friction tests to hope to provide some standardization between labs to allow for experimental repeatability and it is important to choose a test which mimics the use case of the materials as closely as possible. The same material system in different geometric configurations governed by different ASTM standards may provide very different results and even the tests themselves can alter the measurements recorded.[4] Furthermore, the scope of situations covered by the available ASTM tests is limited so many labs, including Lehigh's own, use their own procedures to explore an expanded parameter space beyond those covered by existing standards. The Tribology Laboratory at Lehigh University uses many tribometers designed and built in house to conduct tribological testing in experimental spaces covered by ASTM standards and beyond. As such, it is important to qualify these results to ensure that they are valid. Using uncertainty analysis, it is possible to show the typical separation between the true value of a measurement and the noise and error inherent in any measurement. This allows results to be trusted and shared with the larger scientific community.

Uncertainty

Like tribology, uncertainty is a relatively novel concept. Uncertainty analysis allows for the evaluation of scatter in data measured in an experiment to provide a range of the true value of the measurement.[5] Although the nomenclature relating to uncertainty can be muddy at times, all vocabulary

does have a specific meaning which will now be explained. Whereas manufacturers may quote the repeatability, accuracy, or precision of a measuring device these are all different from uncertainty. Additionally, all of these are different still from error. Reporting of uncertainty requires two values: the interval of the uncertainty and the confidence level of this interval. For instance, a scale could have an uncertainty of 1 gram at a 95% confidence level. This means that you can be 95% sure that a measurement made by the scale will be within 1 gram of the true value.

Measurements are a qualitative property of an object. They are taken by instrumentation and result in both a number and a unit of measurement. An example would be the temperature of a room. This value would be measured by a thermometer, an instrument. The result would be a number, let's say 70, and a unit, such as °Fahrenheit. Thus, the complete measurement would be 70 °F.

Every measurement also has uncertainty inherent in it which can come from many different sources. Uncertainty can be caused by the measuring instruments, the process by which these instruments are used, difficulties arising from the nature of the sample, or the environment. Broadly, uncertainty can be split into either random or systematic errors. Random errors are just that, random. Repeated measurements of value influenced by random error will give randomly different results. These types of errors can be controlled by taking more samples to increase the measurement's sample size. The random errors will then average at least partially out and a more accurate result will remain. Systematic errors are caused by a nonrandom, or bias, error. In these cases, taking additional measurements and averaging them will not remove the error as they are all affected by the bias. However, systematic errors can still be incorporated into uncertainty analysis using different measurement techniques or calculations to figure out the extent of the systematic error and its effect on the measurement's overall uncertainty.

There are two ways to quantify uncertainty through estimation. These two types of evaluations are referred to as either Type A or Type B.[6] Type A evaluations are uncertainty estimations that use statistics on measurements made on an instrument and come directly from experimental data. Type B evaluations use any other information, whether from manufacturer specs or calibrations or elsewhere. One type is not necessarily preferable over the other. Type A evaluations will show the uncertainty of a measurement in

the use case of the actual experimental setup, but the true value of the property being measured is either unknown or known less rigorously than that of a calibration device used by the manufacturer. Type B evaluations on the other hand can sometimes rely on significant judgement calls by the scientist performing the analysis. If the only information about the performance of a measuring device is a brief line about precision or accuracy on a manufacturer's spec sheet an estimate will need to be made about what this means specifically in terms of uncertainty.

Typical Wear Rates and Friction Coefficients

The first step in establishing the suitability of measurement equipment is to assess the typical range of values expected to be measured by the device; you would not buy a ruler to measure the dimensions of a room in your house. Since the two measurements made by the tribometer described in this paper are friction coefficient and wear rate, the literature has been explored to create an idea of typical values for these measurements. Typical friction coefficients vary from nearly 0 to slightly above 1. Wear rates, measured in cubic millimeters per newton meter, typically range from 10^{-2} to 10^{-8}. Most measurements become more difficult to make as their scale decreases and this is also the case with these measurements.

Uncertainty in Tribology

This last graph, Figure ##, illustrates a few points. Friction coefficient values typically range from the order of 10^{-2} to 10^{0}. Wear rates have a much larger range from 10^{-9} to 10^{-3}. Furthermore, this provides a picture of the variability typical of data in tribology. The friction force measurements made in these experiments varies from 7% all the way up to nearly 40%. Wear rates also display a wide variation on the order of half of an order of magnitude of the reported value. From this we can make a decision on an acceptable amount of uncertainty in the measurements reported by the tribometer described in this paper. Uncertainty will be deemed acceptable if it remains below 10% or one order of magnitude of the reported measurement. However, as shown later in the uncertainty analysis, most sources of uncertainty provide

either significantly more or significantly less uncertainty than this threshold so it's value is rather arbitrary in this context.

The wear of materials does not always occur in the same manner. There are several different types of wear mechanisms such as: adhesive, abrasive, surface fatigue, fretting, erosive, and corrosive or oxidative wear.[7] The performance of material systems in these different wear regimes is dependent on many factors and cannot be easily extrapolated from one regime to another. Friction and wear measurements are also strongly affected by lubrication type and methods, environmental factors, and contact conditions.

One source of this variation in testing is the sensitivity of the small measurements of forces required to calculate these values to misalignment in the experimental setup. This is especially true for low friction materials, with some sources claiming measurement of friction coefficients below 0.05 being impossible to resolve with an uncertainty of less than 1%.[8] Thankfully, the multifunctional tribometer allows testing in an experimental space which has been shown to eliminate the effects of misalignment on the measurements.

Reciprocating v Unidirectional Wear Testing

One tool to help control the variability in tribological testing is the use of reciprocating motion for wear testing. This motion is typically harder on materials than unidirectional testing which can help draw out differences between ultra-low wear rate materials and make the measurement of their wear easier.[9] However, the largest improvement made possible by reciprocating motion is the elimination of sample to load cell misalignment as a source of uncertainty in friction measurements. It has been shown that averaging the friction coefficient measurements made during the forward and reverse motion stages of a reciprocating test mathematically and experimentally removes this as a source of uncertainty from the overall value for friction coefficient.[10]

ASTM standards

The multifunctional tribometer is a product of the desire to have a test machine which would be capable of performing many different standardized friction and wear tests while also outperforming commercial machines. The tribometer was designed with significant modularity in mind which allows a core set of components to be repositioned and repurposed to conduct many different standardized tests. These tests fall into several broader categories of test geometries: block on ring, thrust washer, and pin on disc. A variety of test configurations are necessary as friction coefficient and wear rate are system properties which depend not only on the materials used but also the physical geometry they are used in.

Block on Ring

The block on ring geometry is the focus of this thesis. Both the uncertainty analysis and case study utilize the block on ring configuration. Block on ring tests are covered by ASTM standards D2714, G77, G137, and G176, and all follow the same general schematic in Figure 1. The ASTM D2714 standard describes a test using a specific commercial tribometer, produced by Falex, to measure the kinetic coefficient of friction between a steel ring and a steel block lubricated with oil at a normal load of 5 pounds at a speed of 72 RPM.[11] This test is intended to test the efficacy of different petroleum based products and lubricants. The other three standards describe each describe block on ring tests where the laboratory can specify the materials, loading, and rotational speed used. Each test will give wear rate, static friction coefficient, initial kinetic friction coefficient, and final kinetic friction coefficient. These tests differ mainly through their method for measuring wear at the conclusion of the test. ASTM G77 is targeted at metal on metal block

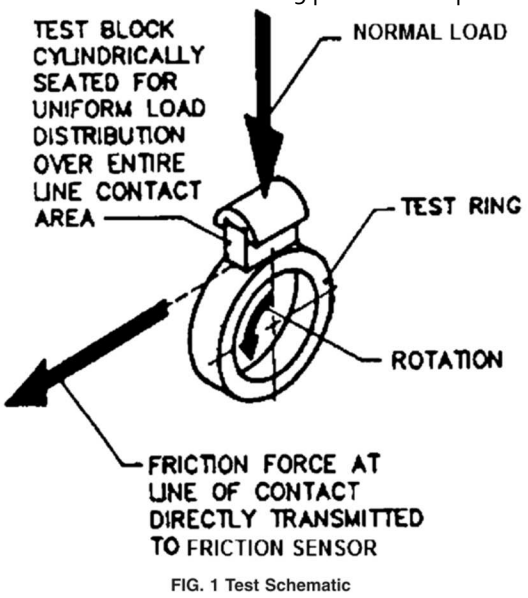

Figure 1: Typical ASTM Block on Ring Schematic

on ring testing and describes using the width of the wear scar to calculate the wear rate of the block.[12] The ring is massed to assess its mass loss over the duration of the test to calculate its wear rate. The block on ring case study included later most closely resembles this ASTM standard. ASTM G137 is intended to test blocks made of plastic.[13] Block wear rate is measured by mass loss. Instead of only a single mass loss measurement at the conclusion of the test, measurements are taken periodically to better establish the wear rate. Wear is often not a linear process and typically involves two stages: run in and steady state. The periodic massing of the block in this test allow these different wear rates to be observed and to observe whether the sample wears linearly or follows another function. ASTM G176 is basically identical to ASTM G77 except it is described as intended for use with a plastic block, but does not describe any differences in testing procedure.[14]

These ASTM standards also list some basic sample parameters which we try to adhere to for experiments conducted with parameters expanded beyond these standards as good practice for tribological testing. However, the parameters provided by the standards do not always overlap and some are missing entirely. A summary of all the parameters specified in the ASTM block on ring standards is shown in Table 1: ASTM Block on Ring standards summary. It is clear from this table that these standards do not cover close to all experimental spaces that can be explored with the multifunctional. Therefore, it is necessary to use these as rough guidelines for use with the reciprocating tests enabled by the multifunctional tribometer which include the following specifications. A maximum eccentricity/run out for each mounted ring is specified at .00125mm. The rings themselves are specified as having an outer diameter of 34.99mm ±.025mm. Roughness for the ring's outer surface should be a ground surface with an R_q between .152 to .305µm. The test block should be 6.35 +0.000, -0.025mm wide with its testing surface ground parallel to the direction of wear testing to a roughness of R_q 0.102 to 0.203µm.

Specification	G176	G137	G77	D2714
Ring Outer Diameter (mm)	34.99 ±0.025	100. -0., +0.05	34.99 ±0.025	35
Ring Width (mm)	---	15.88 -0.13, +0.30	---	8.15
Ring Eccentricity (mm)	0.00125	±0.06	0.00125	0.013
R_q Ring (µm)	0.152 - 0.306	0.102 - 0.203	0.152 - 0.306	0.15 - 0.30
Block Width (mm)	6.35 -0.025, +0.	6.35 -0.03, +0.	6.35 -0.025, +0.	6.35
Block Height (mm)	---	12.70 ±0.2	---	15.76
Block Depth (mm)	---	6.00 -0.03, +0.	---	---
R_a (µm)	---	0.102 - 0.203	---	---
R_q (µm)	---	---	---	0.10 - 0.20
R, type not specified (µm)	---	---	0.102 - 0.203	---
F_N (N)	44.3	20. - 40.	Apply 133N every 200 revolutions until desired load is reached	667
Speed of Rotation (rpm)	200.	95.5 - 191 *calculated from m/s	---	72 ±1
Length of Test (revolutions)	240000	---	---	5000
Type of Motion	Unidirectional	Unidirectional	Unidirectional	Unidirectional

Table 1: ASTM Block on Ring standards summary

Block on ring tests can either use line or conformal contact samples. An example of each type of sample is shown in Figure 2: Left: line contact, Right: conformal contact. Additionally, Figure 3: Block on ring contact geometries shows other possible contact types that can be utilized including pin on ring and ball on ring. The range of contact pressures achievable in block on ring testing is increased through the application of these different contact geometries, and also allow for closer matching between laboratory testing and a wider range of real world

Figure 2: Left: line contact, Right: conformal contact

applications. Conformal tests better model the wear seen in the bushing applications including anything from roller chains to door hinges.

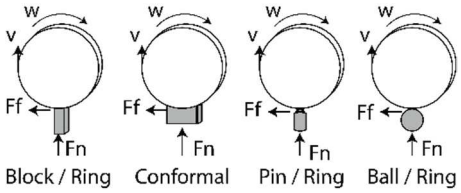

Figure 3: Block on ring contact geometries

In addition to different contact geometries, differences in the type of motion of the sample can be realized. ASTM testing standards only cover unidirectional testing, but there are many cases of bushings being used in reciprocating applications. As discussed previously, reciprocating motion not only provides benefit to the robustness of data quality and acquisition but also allows for more accurate modeling of these additional application spaces. Therefore, these tests are necessary and valid even if not covered by ASTM standards.

Thrust washer

The thrust washer geometry is defined in the D3702 ASTM standard. In this test contact the contact geometry is flat on flat, created by two washer shaped samples being pressed into contact, shown in Figure 4. In addition to this specific test the tribometer is also capable of performing reciprocating and unidirectional wear tests across a wide range of test conditions. With exception of the reciprocating testing mode these test procedures were developed prior to the work undertaken in this thesis and therefore will not be covered in as much detail.

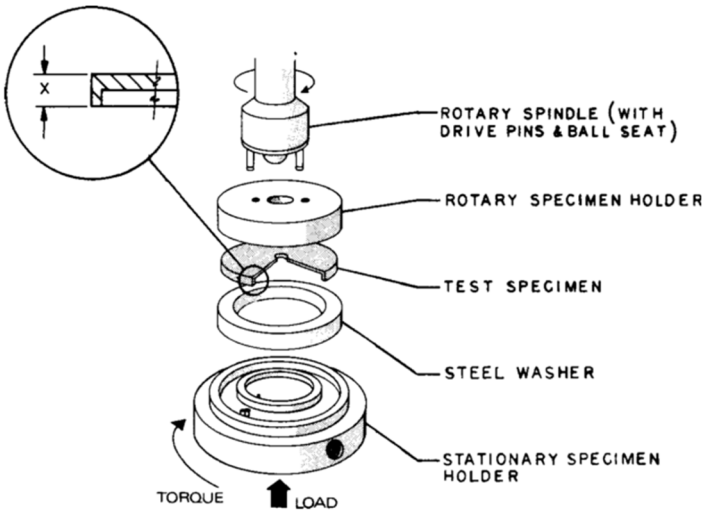

Figure 4: ASTM Thrust Washer Schematic

ASTM D3702 describes a specific test to evaluate the wear rate and friction coefficient of self-lubricating materials. [15] To follow this standard tests must have a contact area of 1.29 cm^2 and be run at a spindle speed of 1rpm. Load application is by dead weight acting

on a lever arm and all tests are subject to a 40-hour break in period before data collection begins. Wear rate is reported in centimeters per hour for the thickness of the test specimen along with the torque required to spin the sample to calculate coefficient of friction.

Obviously, this ASTM standard is very limited in its scope. The multifunctional tribometer is capable of using both reciprocating or unidirectional motion. Also, there is a provision to conduct lubricated tests along with dry testing. Rotational speed can be varied from below one revolution per minute to above 3000 revolutions per minute.

Planar alignment between the test specimen and steel washer is very important. In order to accommodate this misalignment, the ASTM standard recommends mounting the sample on a pivoting surface, also shown in Figure 5. The multifunctional tribometer uses a very similar configuration to mount test specimens that uses the same principle of pivoting around a ball and is shown in Figure 5. This is referred to as the gimbal and it allows for the correction of slight misalignment between the sample surfaces by allowing the steel washer to pivot on top of a ball bearing while remaining constrained in rotation by small screws at the corner of the gimbal plate. This allows the specimen to tilt, but not spin while tests are run.

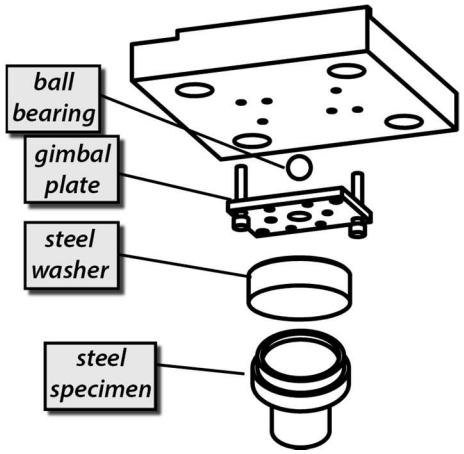

Figure 5: In house gimbal design

The configuration of the tribometer differs between the block on ring and thrust washer testing regiments. Figure 6 shows how the pneumatic thruster is repositioned to be coaxial with the spindle in order to wear the face of the sample instead of its side.

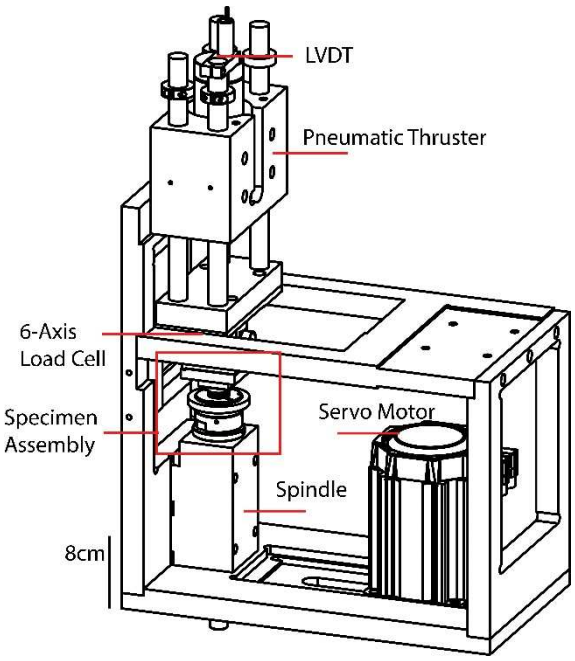

Figure 6: Multifunctional tribometer thrust washer configuration

Multifunctional Tribometer Overview

The tribometer utilized in this paper is referred to as the multifunctional tribometer. This is because it is capable of being utilized in multiple configurations to conduct experiments in many different testing geometries. The basic building blocks of the tribometer, some of which are rearranged for different experiments, are as follows: the frame, thruster, spindle, motor and controller, and load cell shown in Figure 7.

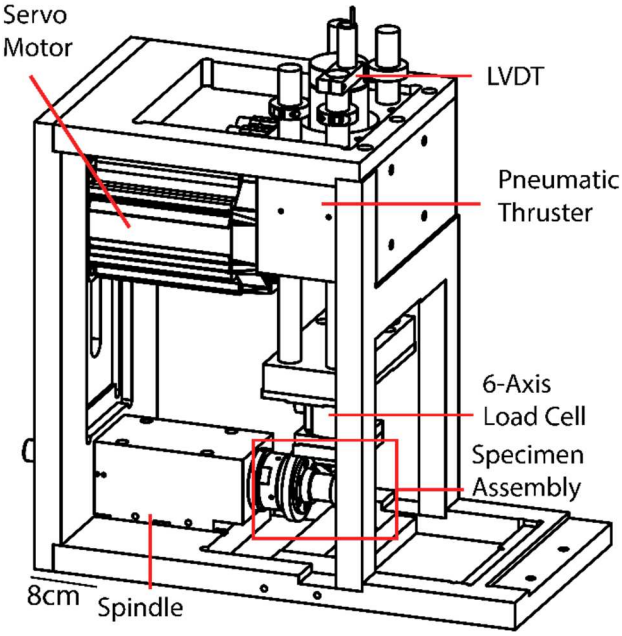

Figure 7: Tribometer in block on ring configuration

The frame is made from four pieces of aluminum and was designed to ensure high rigidity and correct alignment between all components of the tribometer. As will be discussed later in this report, alignment of test components is critical to ensure accurate measurements. To achieve highly accurate and repeatable alignment in the machine components are located using alignment ledges in lieu of bolts. These ledges, as a form of kinematic mount, ensure that as components are rearranged and reconfigured during the different testing regimes of the tribometer that they will always be well aligned.

One measurement required to calculate both friction coefficient and wear rate is the normal force applied to the material interface. As such, this force needs to be easily applied and varied. A pneumatic thruster, shown in Figure 8 was chosen for this purpose due to its ability to be electronically controlled through the use of electropneumatic valves. It can also apply force anywhere through its considerable

stroke, 6 inches on this instrument. Finally, this pneumatic thruster can apply a force ranging from nearly 0 N to 2180 N, providing additionally testing flexibility.[16] This range is limited by the pressure of the air fed to the thruster and thus could be increased further through the use of higher pressure air.

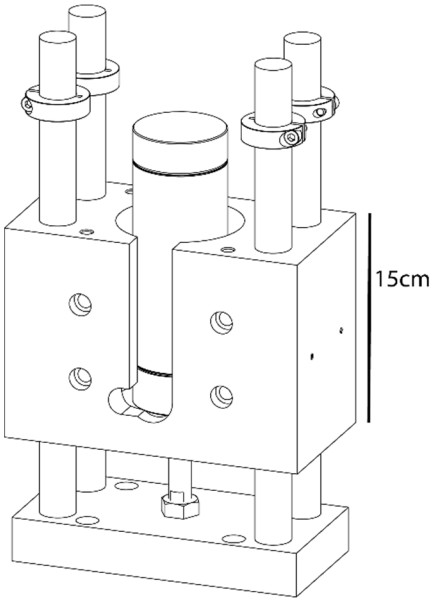

Figure 8: Pneumatic thruster

The multifunctional tribometer conducts mainly rotational tests and thus needs a spindle and motor to rotate samples. The motor and controller both come from Parker. The motor, shown in Figure 10, is a MPJ1422C1E-KPSN which is controlled by a Compax3 S150V2F12I11T30M00 controller. These two components combined allow for a 3.40kW motor capable of outputting up to 10.9 Nm of torque or spinning up to 4300RPM which is controlled through either serial commands, analog voltages, or internal PLC programming.[17,18] In the block on ring configuration the motor controller is programmed to use PLC programming, but in thrust washer testing it is configured to output a specific torque based on an analog input voltage ranging from 0v to 10v. This motor spins a Gilman Precision 2750-30 spindle, depicted in Figure 9, which can run up to 10400 RPM with a maximum thrust loading of 1286N.[19] This thrust loading rating provides the limit for the application of normal force in thrust washer and pin on disc testing. Additionally, the spindle radial stiffness is rated at 36777 N/mm, which at the maximum loading possible on this tribometer results in a displacement of .059mm. At more typical loadings, this displacement goes down to under .014mm.

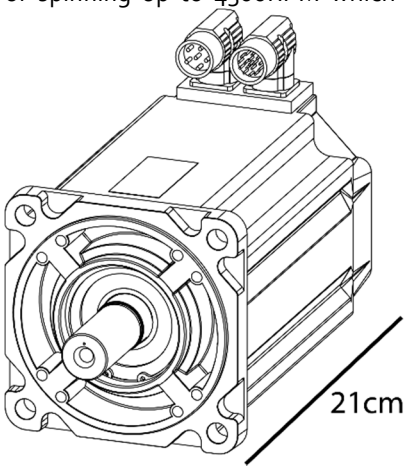

Figure 10: Parker MPJ series motor

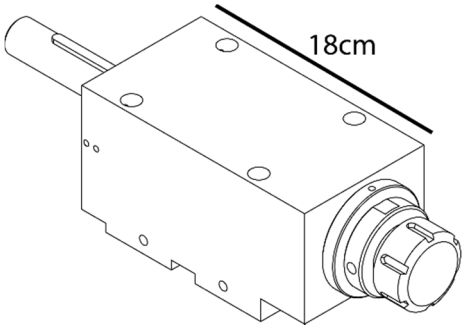

Figure 9: Tribometer spindle

Finally, the multifunctional tribometer is equipped with instrumentation to measure the various components necessary to calculate friction and wear rate. The main piece of this instrumentation is the multidimensional load cell, an AMTI MC3A-500, shown in Figure 12. This load cell is capable of measuring force and moments in 6 axes: X, Y, and Z; and the moment about X, Y, and Z. Force and torque capacities are as follows:1112N in the X and Y directions, 2224N in the Z direction, 56Nm around the X and Y axes, and 28Nm around the Z axis.[20] This allows for the simultaneous measurement of torque, normal load, and frictional force as demanded by each experiment. The load cell experiences deformation during use; this is how load cells function. Figure 14 and Figure 15 show the typical deformation of the load cell during typical use in the tribometer in both the thrust washer and block on ring geometries. Both use cases are well within the performance envelope of the thruster as is shown in Figure 13 and Figure 16. The green rectangles represent the typical use case of the thruster during experiments which are well below the black line representative of the rating of the thruster. Deformation will be experienced in the Z and M_z axes for thrust washer experiments and the Z and X/Y axes for block on ring testing. The load cell is very still and the deformation experienced during testing is on the order of a few hundredths of a degree and a few microns. Additionally, the tribometer is equipped with an LVDT, which measures displacement and is shown in Figure 11. This is used to help calculate the volume loss of a sample during testing which is a value integral to calculating wear rate. Here specifically, a DCTH300AG LVDT produced by the RDP group is used.[21] This model has a useful measurement range of 15mm and combined with our DAQ system can be used to accurate measurement changes in displacement

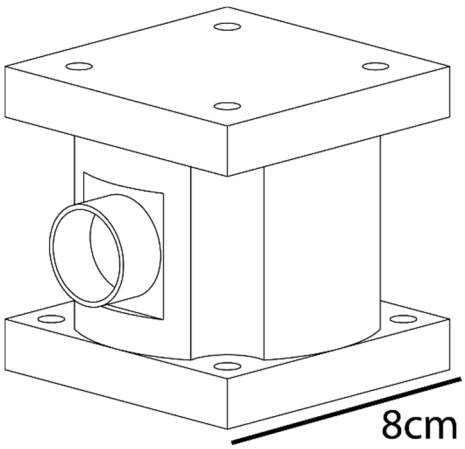

Figure 12: Load cell

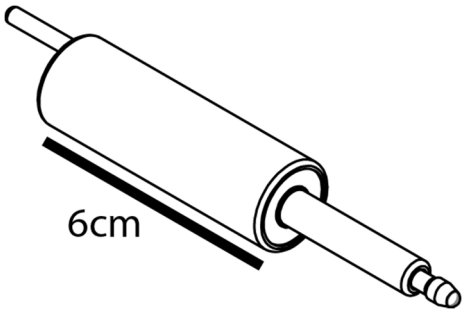

Figure 11: LVDT

on the order of .01mm. The signals from the load cell are then fed into an amplifier to raise the millivolt range signals it outputs into a range between -10 to 10 volts usable by our data acquisition system.

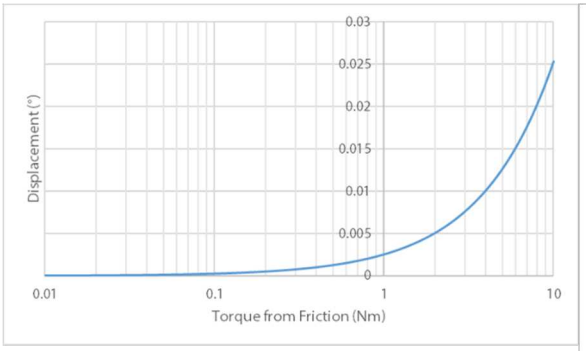

Figure 14: Thruster rotational deformation during testing

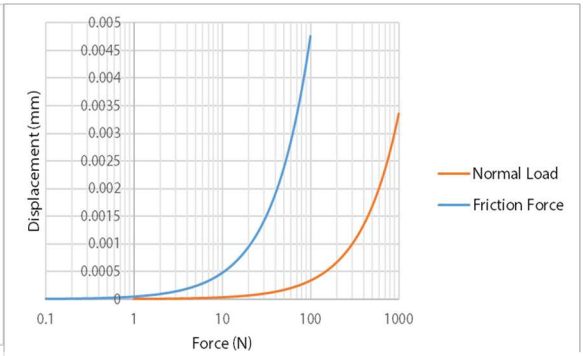

Figure 15: Thruster linear deformation during testing

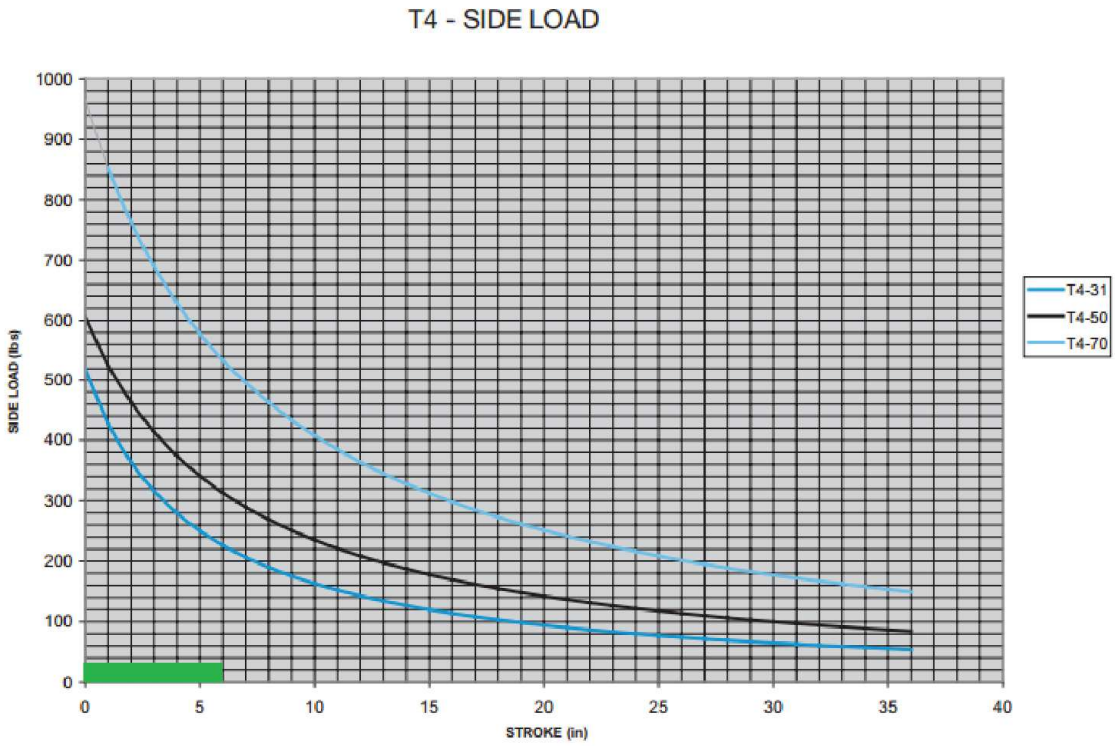

Figure 13: Linear load capacity performance envelope of tribometer

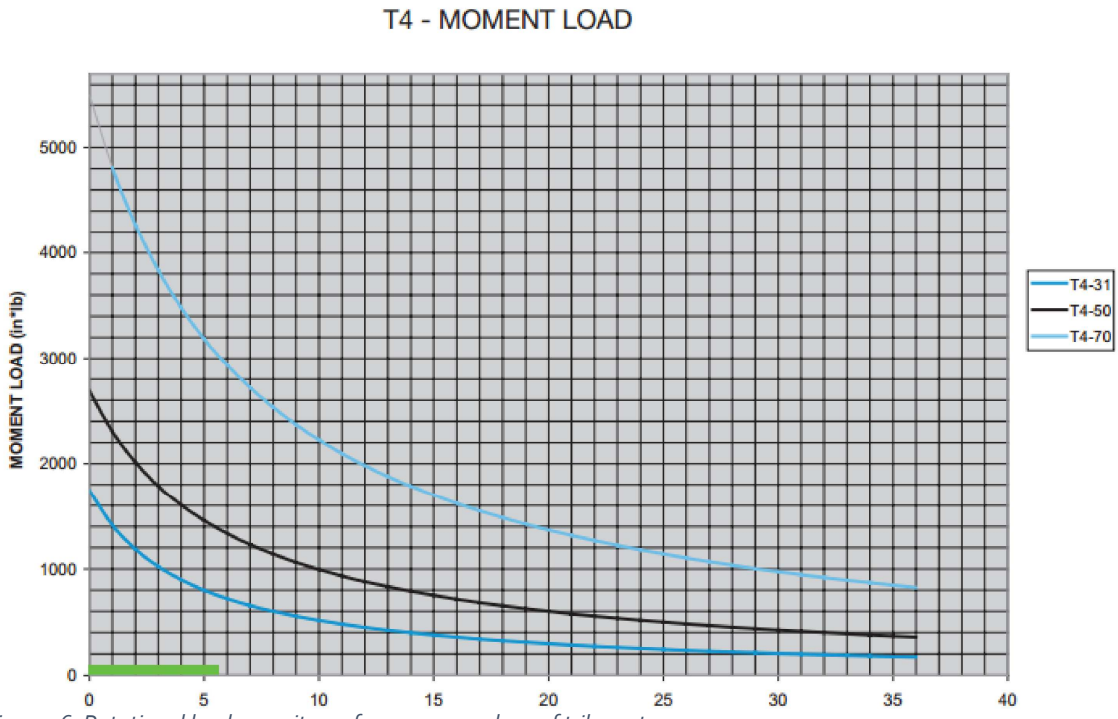

Figure 16: Rotational load capacity performance envelope of tribometer

The tribometer interfaces with computer which both controls it and processes all data produced by experiments. The software interface is provided by several MATLAB programs developed in house. On the hardware side, data and control inputs and outputs are handled by a National Instruments NI-6321 and a National Instruments NI-6009 digital acquisition devices. All data signals are fed into to NI-6321 which provides 16-bits of resolution on its analog to digital conversions.[22] The NI-6321 also supports hardware decoding of an encoder which is utilized on this tribometer. The NI-6009 is used to supplant the analog outputs of the NI-6321 to control the electropneumatic valves used to control the thruster. The motor is controlled using a variety of schemes depending on the experiment being run. Reciprocating experiments use ladder logic to precisely control the rotation of the motor. The motor can also be commanded to spin at a certain RPM or to apply a constant torque depending on an analog voltage; these control schemes are used for a variety of thrustwasher tests

Test Specimen Manufacturing

A significant amount of thought was put into the creation of sample and counter sample mounting. This geometry is very sensitive to alignment issues, especially in the case of noncompliant samples such as metal on metal contact. Of chief importance is creating a correctly aligned and parallel block to ring contact. This is achieved through the careful control of degrees of freedom in the block holder. The design of the block holder is shown in Figure 17. This block holder is designed to allow the block to pivot to create parallel contact with the ring. By carefully controlling the amount of clamping force applied to the block holder the block can rotate while a test is being run to ensure this contact remains parallel even if the ring has some intrinsic amount of wobble. The curvature on the interface between the block holder and the rocker base is designed so the instant center of this rotation lies on the interface between the block and ring. Such a design eliminates the up and down motion that would otherwise be caused by the block rocking on its mount which would manifest itself as a variation in the normal force variation recorded by the tribometer.

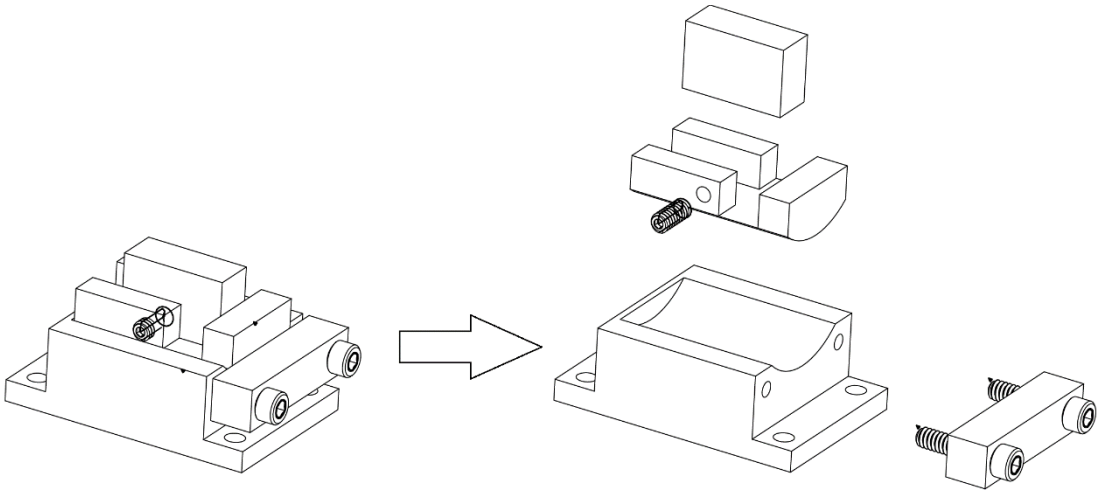

Figure 17: Assembled and exploded views on block holder

It is also of great importance to minimize the eccentricity of the ring. This eccentricity manifests itself as a variation in the normal force reading during testing. The basic mounting system for rings has remained unchanged throughout the instrument's development: rings mount on a tapered spindle. Initially we

purchased rings that came already machined and finished. Unfortunately, these rings are designed to be used on a proprietary testing machined and so details about their design were unavailable to us. Specifically, this caused a problem as we were unable to accurately measure the taper and it did not seem to comply to any common industry standard tapers. This resulted in a poor fit between our in-house manufactured spindle and the commercially sourced rings. Additionally, these rings were expensive and would have strained our budget. Considering these factors, we decided to make rings in house. We then embarked on a long development process to ensure that all tests remained under the ±.00125mm runout called for in several ASTM standards. The fruit of this labor resulted in several design changes. The rings are now taller providing more contact area for the taper, shown in Figure 18. This taper is now one of our own design so its dimensions and angle are exactly known and can provide the level of torque transmission and alignment required.

Figure 18: Left: commercial ring, Right: in house ring design

Block and Ring Manufacturing

The rings are manufactured in a two-step process using CNC machining equipment. The machines utilized for this are provided by Lehigh University and are a HAAS CNC controlled lathe and a HAAS VF2 CNC controlled milling machine. First, stock is loaded into the lathe and turned down to an outer diameter .005" larger than is finally desired. Next, a taper is cut on the interior of the ring. The ring is then parted off

and the next ring blank can be made. The CNC lathe is configured to auto feed new pieces of stock so approximately fifteen ring blanks can be made in a row before human intervention is necessary. After this process the ring blank is moved to a mill where a finishing step takes the ring down to its final diameter using an end mill. This two-step process ensures that surface finish and concentricity of the ring's taper and outer surface are maximized. The mill is utilized for the finishing pass as it is capable of creating a much finer finish than the as turned finish. Concentricity is ensured by mounting the ring blanks in the mill using a tapered arbor that is machined in place on the mill. Rings are then mounted to this arbor and undergo finish machining. As the mill is easily capable of repeatable positioning anywhere on its travel range with .0001" accuracy this process ensures that the taper and testing surface of the ring will have an eccentricity smaller than this amount.

The result of this careful manufacturing is shown in Figure 19. These scanning white light interferometry images compare the surfaces of the commercially available rings, rings made with the previously described process, and rings produced solely using a lathe. Clearly, both the current ring design and the Falex rings surfaces are more uniform than the turned rings. Both the in house manufactured ring and the Falex ring display similar roughness and similar machining marks. Therefore, the rings manufactured in house are comparable to commercially available rings at a fraction of the cost. Also, as an interesting side note, even though the ring in every ASTM is specified to have an rms surface roughness value of below 0.2 µm, the ring measured here has an rms surface roughness of 0.806.

Initially, blocks were manufactured from any available steel stock. Blocks were then machined several at a time by hand on a mill. This resulted in a large variation in size between each block. Blocks now

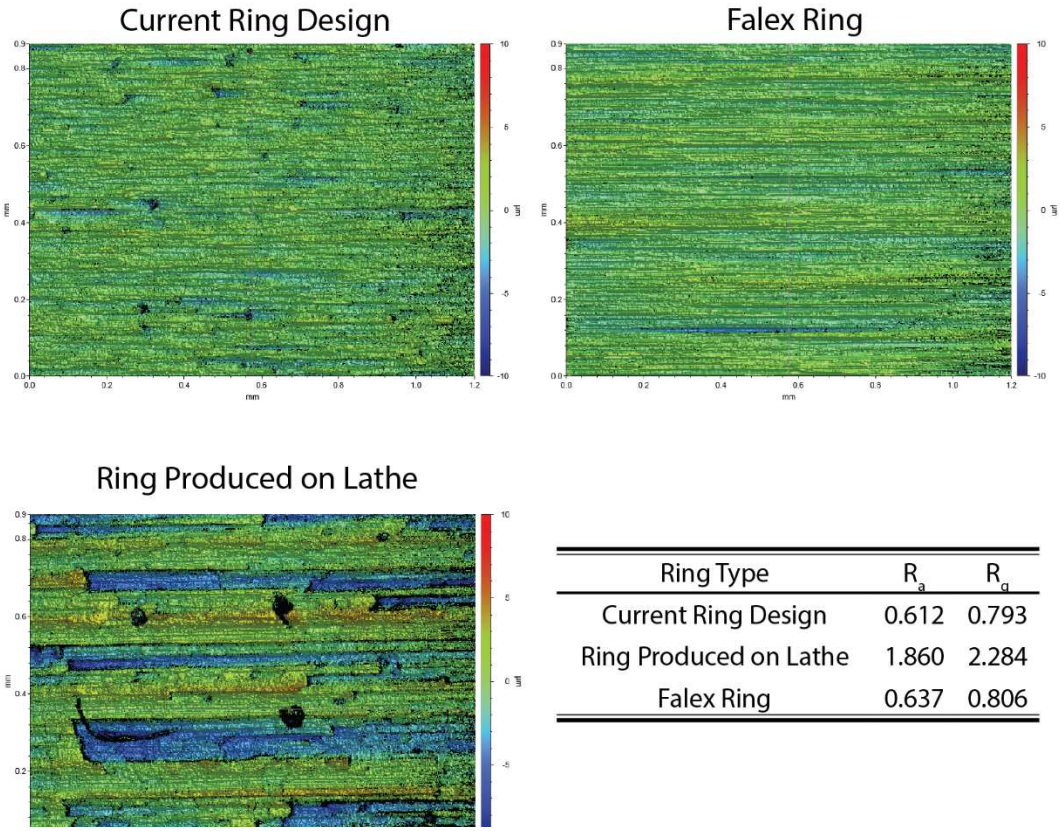

Ring Type	R_a	R_q
Current Ring Design	0.612	0.793
Ring Produced on Lathe	1.860	2.284
Falex Ring	0.637	0.806

Figure 19: Ring surface scan comparison

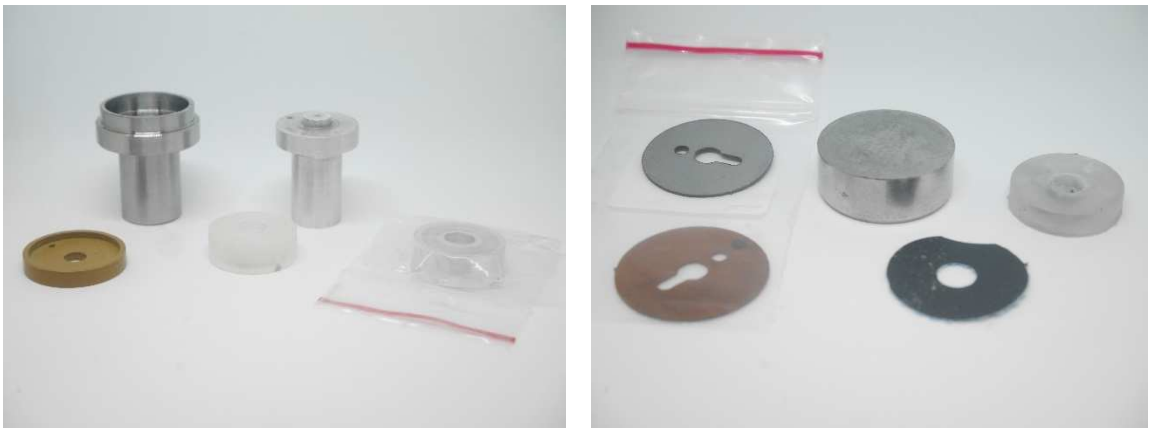

Figure 20: Thrust washer samples and countersamples

begin life as a mass produced standard sized machine key which are specified to a tolerance of less than .001". The machine keys can then be ground en masse for use as blocks.

The common theme for improvements in sample manufacturing is to reduce the time to manufacture each sample. As tribology has high variability in its data it is necessary to test a large sample set. Therefore, if each sample can be prepared quicker then more tests can be conducted. These improvements have decreased the time to make a single block and ring from around an hour of manual, skilled machining to a couple minutes per sample which are machined totally using numerical control milling and turning.

Thrust Washer Manufacturing

A variety of samples and countersamples can be used depending on the characteristics desired in the experiment. Samples can either be shaped to directly mount inside the tribometer's spindle, or can be made to fit on a mandrel which is in turn mounted to the spindle. Counter samples can either mount directly to the load cell, mount to a gimbal as shown previously, or mount to a compliant surface which is attached to the load cell. A variety of samples and counter samples are shown in Figure 20.

Uncertainty analysis

Overview

Wear rate and friction coefficient are the two most important values derived from this tribometer and as such these values are the target of this uncertainty calculation. Before delving into this analysis, it is beneficial to discuss the framework used to analyze each individual contribution to uncertainty.

Explanation of Format

The information related to each component and its uncertainty will be presented in a format similar to that in Table 2. The uncertainty analysis is divided into a different category for each value necessary to calculate either wear rate or friction coefficient. These sections may then be further broken down if these values are themselves calculated values and not direct measurements, as is the case for volume loss of the block. Each category of uncertainty will then have another table which shows each of these sub tables' contribution to that measurement's uncertainty.

Each component of that measurement's uncertainty will have a row in the table and several of these values depend on the mean or typical value of the measurement in the prototype experiment. The first column in the table is the source of uncertainty being evaluated, here it is the accuracy of the calipers used to measure the width of the block. Then comes the typical or mean value of the measurement from the experiment which varies depending on the experiment being run and the measurement being made. Next comes the uncertainty caused by this source of error; this value is unaffected by the mean value chosen. Fourth is the percent of the total uncertainty in the value or measurement being evaluated in the

Source	Typical Value (mm)	Uncertainty (mm)	% of Uncertainty	% of Typical Value
Caliper Accuracy	6.31	0.0231	64.8%	0.36%
Block Width		**0.0283**		**0.448**

Table 2: Example uncertainty analysis results

Parameter	Value
Block Dimensions (mm)	6.312 x 6.027 x 18.707
Block Volume Loss (mm^3)	$4.19x10^{-8}$
Ring Radius (mm)	17.721
Ring Density ($g/m^{3)}$	$7.87x10^6$
Friction Force (N)	100

Table 4: Additional typical values

section of the uncertainty analysis; here it is the width of the block. Finally, the uncertainty is compared to the mean value of the measurement shown in column 2 of the table.

The bottom line of each table is the actual measurement or value needed for the calculation of wear rate or friction force. This is named in each section of the analysis and again in the first column of the table. Next is the total uncertainty in this measurement or value being calculated. If the table relates to a measurement, then the uncertainty is unaffected by the mean value chosen. However, if this is a calculated value, then it is dependent on the typical values pulled from the prototype experiment.

Experimental Method

As was mentioned previously, some calculations in this uncertainty analysis require the knowledge of the mean value of a measurement in an experiment. For this analysis, these values are referred to as the experimental method. This experiment, the results of which are discussed in depth later in this paper, is a block on ring experiment conducted using the parameters in Table 3. Other mean values used include the dimensions of the block and ring, the volume lost by these during testing, and the friction force measured during testing, the values chosen for each are displayed in Table 4. For clarification on the meaning of stroke in the experimental parameters please see Figure 21 which depicts a reciprocating

Parameter	Value
Normal Force (N)	500
Speed (rev/s)	2
Stroke (°)	360
# of Cycles	100
Lubricant	WD40 MUP

Table 3: Prototype experiment parameters

motion with a stroke of 90°. First the ring moves 90° clockwise, then it returns to the starting position by moving 90° in the counterclockwise direction. The motion in this experiment is similar except the ring moves 360° in each direction.

Coverage Factor and Type B Analyses

Uncertainties also depend on a coverage value which is analogous to the number or standard deviations used to define the width of a confidence interval. All values for uncertainty in this paper use a coverage factor of 2. This means that you can be 95% sure that a measurement's true value is within the value of the uncertainty of the measured value. This coverage factor is denoted in equations as c instead of the more typical k so as to not be confused with wear rate, K.

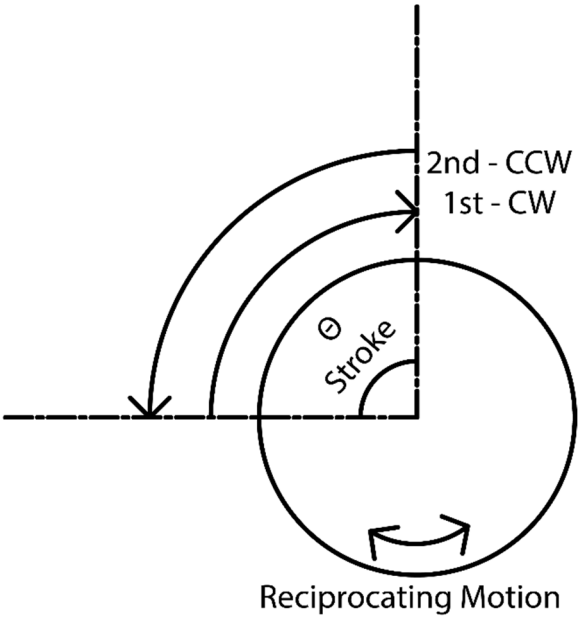

Figure 21: Schematic of the meaning of stroke

Type B uncertainty analyses, those which are calculated from manufacturer's specifications or anywhere except from actual data recorded by the instrument, are modeled here as having a rectangular distribution. This allows the uncertainty provided by these manufacturer's specifications to be estimated using the following formula, where u is the uncertainty resulting from the distribution and a is the half width of the interval:

$$u = \frac{a}{\sqrt{3}} \tag{1}$$

A graphical representation of what this means is shown in Figure 22. This approach was chosen as it does not rely on any outside decision making by the individual conducted the uncertainty analysis. Additionally, it provides the highest standard deviation and uncertainty of any shape of distribution.[23] This conservative approach should therefore provide more repeatable values for uncertainty between separate analyses.

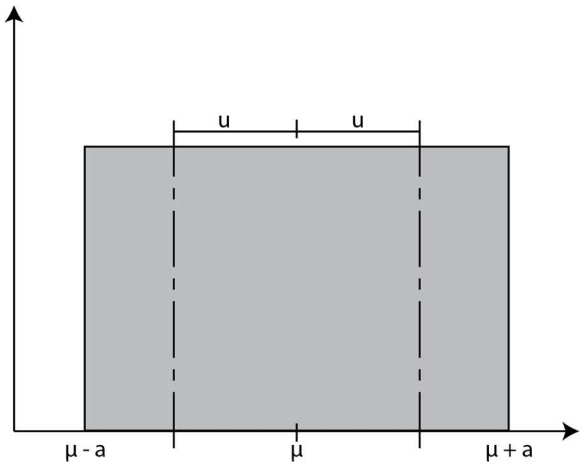

Figure 22: Explanation of the uncertainty in a rectangular distribution

Mass Loss (ring)

Mass loss is used to calculate the wear rate of the ring. This method is one of the simplest way to calculate wear rate, but it comes at the cost of higher uncertainty. This arises from the difficulty of measuring such small changes in mass, especially in a metal sample with its corresponding low wear rate. Mass loss is calculated, simply enough, using the following formula:

$$\Delta m = m_f - m_i \tag{2}$$

An initial measurement, m_i, of the mass is made, and then following the conclusion of the test a second measurement, m_f, is made of the ring's final mass. The difference of these two measurements is the mass loss, Δm. From this follows the derivation of the uncertainty in this measurement:

$$u_c(\Delta m) = c\sqrt{u\left(m_f\right)^2 + u(m_i)^2} \tag{3}$$

The uncertainty in the final and initial mass losses are equal and are each also calculated from the root sum of squares of each contribution to the uncertainty in the mass measurement.

The scale used in these experiments is a Mettler Toledo XS205 which has a claimed repeatability of +/-.02mg and a resolution of .01mg.[24] The uncertainty in the mass loss has also been calculated in two ways: using a type A and a type B analysis. Furthermore, these contributions to the total uncertainty of this

measurement must be double counted as two measurements must be made to calculate the mass loss. This increases the uncertainty compared to a single measurement by a factor of $\sqrt{2}$. The type B calculation uses the manufactured provided data for the repeatability and resolution of the scale and these results are shown in **Error! Reference source not found.**.

Source	Typical Value (g)	Uncertainty (g)	% of Uncertainty	% of Typical Value
Scale Repeatability	0.1	3.27×10^{-5}	20.0%	0.03%
Scale Resolution	0.1	1.63×10^{-5}	80.0%	0.02%
Mass Loss (Ring)		**5.16×10^{-5}**		**0.05%**

Table 5: Type B uncertainties for ring mass loss

We wanted to ensure that during typical use of the scale its repeatability is on par with the value reported by the manufacturer. As such, a quick set of repeated measurements was conducted to use this data for a Type A uncertainty analysis, shown in **Error! Reference source not found.**. Each measurement as made by placing the ring on the scale, waiting for the value on the scale to become constant, noting the mass, then removing the sample. After these values were recorded a sample mean, standard deviation, and uncertainty were calculated, which are shown in Table 6.

# of Samples	Average Mass (mg)	Standard Deviation (mg)	Uncertainty (mg)
10	39294.48	0.0939	0.0599

Table 6: Experimental data on scale repeatability

This new data was then incorporated into the previous uncertainty calculation and the result is shown in Table 7. While there is a small increase in total uncertainty of the mass loss measurement, it still remains the most accurate method to determine volume loss and hence wear rate compared to direct measurement with an LVDT or surface scanning techniques.

Source	Typical Value (g)	Uncertainty (g)	% of Uncertainty	% of Typical Value
Scale Repeatability	0.1	3.27×10^{-5}	22.10%	0.03%
Scale Resolution	0.1	1.63×10^{-5}	5.53%	0.02%
Typical Use	0.1	5.91×10^{-5}	72.37%	0.06%

Table 7: Ring mass loss uncertainty, including errors introduced from typical use

Volume Loss (block)

In contrast to the previous method, the wear rate of the block is computed using knowledge of geometry along with the displacement of the block relative to the ring as the block wears down. As explained previously, this measurement is made possible with the use of an LVDT and assumes that the ring will wear a circular wear scar in the block of the same dimension as the ring. A schematic of the geometry is shown in Figure 23: Schematic of circular segment which depicts the profile view of a ring wearing into a block. This creates a shape known as a circular segment. The area of this segment can be found with the following formula[25]:

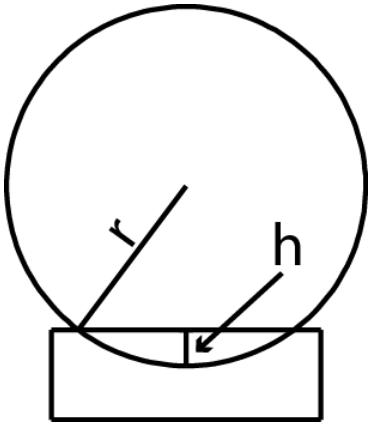

Figure 23: Schematic of circular segment

$$A = r^2 \cos^{-1}\left(\frac{r-h}{r}\right) - (r-h)\sqrt{2rh-h^2} \quad (4)$$

This is valid if it is assumed the ring will wear away a volume of the block in the same shape as itself. This value for cross sectional area is then multiplied by the width of the block to find the volume loss of the block.

Calculating the uncertainty of the volume loss in this manner requires a combination of type A and B analyses. Type B analyses are necessary for the caliper used to measure the width of the block and the radius of the ring, the LVDT, and the data acquisition system. The caliper used is a Mitutoyo 500-196-20 with a claimed accuracy of +/-.02mm, repeatability of .01mm, and resolution of .01mm.[26] In addition to these values are several Type A uncertainties which needed to be accounted for and incorporated into the overall block volume loss uncertainties. These included the noise in the data acquisition system, and the variability of the width of the blocks and radius of the rings. The inclusion of the variability of the blocks and rings used allows for the evaluation of whether it is necessary to individually measure these values of each sample before running each experiment or if overall uncertainty will remain low enough to render this additional information and corresponding lowered uncertainty unnecessary.

To gather the information necessary for these Type A analyses, experimental data was collected to characterize various errors inherent in the tribometer and experimental samples. The noise present in the data acquisition system was evaluated first. This was done by applying recording 1000 values for each analog input channel used by the DAQ with the corresponding devices attached and turned on, but without any changes that would cause their output to value for any reason other than noise. These results are shown in Table 8 and while this uncertainty is a large contribution to the overall uncertainty of the block's volume loss, it is undoubtedly better than using the laboratory scale to make a measurement of mass loss.

Next we measured the variation in the physical size of both the blocks and rings. Taking 16

# of Samples	Mean Displacement(mm)	Standard Deviation (mm)	Uncertainty (mm)
1000	5.92	0.01984	0.00177

Table 8: Experimental data on DAQ noise while measuring LVDT data

different samples of each and measuring the width of the blocks and radius of the rings gave the following results shown in TABLE###. Variability is understandably low due to the tightly controlled manufacturing of these samples and bodes well for their contribution to overall uncertainty.

Source	Mean (mm)	Standard Deviation (mm)	Uncertainty (mm)	% of Mean
Block Length	18.71	0.0843	0.0422	0.02%
Block Width	6.31	0.00952	0.00476	0.23%
Block Height	6.03	0.00765	0.00382	0.08%
Ring Radius	12.72	0.00544	0.00272	0.06%

Table 9: Measurement of variability in blocks, n = 16

Now it is necessary to derive another equation which describes the total volume loss uncertainty.

$$V_L = W \times A \tag{5}$$

$$u_c(V_L) = c\sqrt{\left(\left(\frac{\partial V_L}{\partial W}\right)^2 u^2(W) + \left(\frac{\partial V_L}{\partial A}\right)^2 u^2(A)\right)} \tag{6}$$

$$u_c(V_L) = c\sqrt{\left(\left(\frac{\partial V_L}{\partial W}\right)^2 u^2(W) + \left(\frac{\partial V_L}{\partial r}\right)^2 u^2(r) + \left(\frac{\partial V_L}{\partial h}\right)^2 u^2(h)\right)} \tag{7}$$

$$\frac{\partial V_L}{\partial h} = W\left(\frac{r}{\sqrt{1-\frac{(r-h)^2}{r^2}}} + \sqrt{2rh-h^2} + \frac{(r-h)h}{\sqrt{2rh-h^2}}\right) \tag{8}$$

$$\frac{\partial V_L}{\partial r} = W\left(2r\cos^{-1}\left(\frac{r-h}{r}\right) - \frac{r^2\left(\frac{1}{r}-\frac{r-h}{r^2}\right)}{\sqrt{1-\frac{(r-h)^2}{r^2}}} - \frac{h(r-h)}{\sqrt{2rh-h^2}}\right) \tag{9}$$

$$\frac{\partial V_L}{\partial W} = A \tag{10}$$

As shown in these equations, in order to calculate the uncertainty in volume loss it is necessary to individually calculate the total uncertainty in the block width, the radius of the ring, and the wear scar depth. Additionally, these steps will allow us to evaluate the effect on the uncertainty if each individual block is not measured for width and each ring is not measured for its radius. If assuming the mean value for these values instead of their actual values still returns a low uncertainty for the block's volume loss, then some time savings in the experimental procedure can be realized by skipping these steps.

Block Width Uncertainty

The uncertainty in the width of the block is governed by the uncertainty in the calipers used to directly measure the width along with manufacturing tolerances of the block itself. The calculation is again the root sum of squares of each contribution to the uncertainty of the measurement which are shown in Table 10. Omitting the individual measurement of the width of each block produces an increase of uncertainty of only 0.0006% in the uncertainty of the block width, which is itself only one component of the overall uncertainty of the block's volume loss. Therefore, it is reasonable to say that individual

measurement of each block's width is unnecessary using the manufacturing methods used to create these blocks.

Source	Mean Block Width (mm)	Uncertainty (mm)	% of Uncertainty	% of Mean
Caliper Resolution	6.31	0.0115	16.2%	0.18%
Caliper Accuracy	6.31	0.0231	64.8%	0.36%
Caliper Repeatability	6.31	0.0115	16.2%	0.18%
Block Width Variation	6.31	0.00476	2.76%	0.08%
Block Width (individual block width measurements)		**0.0283**		**0.448%**
Block Width (typical block width assumed		**0.0287**		**0.454%**

Table 10:Block width uncertainty, with and without errors introduced from assuming individual block width

Ring Radius Uncertainty

The uncertainty calculation for the ring radius is identical to that for the width of the block except it includes the actual ring diameter uncertainty instead of that for the block width. From Table 11 it is evident, again that measuring the radius of each individual ring is unnecessary; providing a 0.001% reduction in the uncertainty of this part of the overall block volume loss uncertainty.

Source	Mean Radius (mm)	Uncertainty (mm)	% of Uncertainty	% of Mean
Caliper Resolution	12.72	0.0115	16.5%	0.09%
Caliper Accuracy	12.72	0.0231	66.1%	0.18%
Caliper Repeatability	12.72	0.0115	16.5%	0.09%
Ring Radius Variation	12.72	0.00272	0.92%	0.01%
Ring Radius (individual ring radius measurements)		**0.0283**		**0.222%**
Ring Radius (typical ring radius assumed)		**0.0284**		**0.223%**

Table 11: Ring radius uncertainty, with and without errors introduced from assuming individual ring radius

Wear Scar Depth Uncertainty

The third piece of information necessary is the uncertainty in the wear scar depth measurement. These calculations assume the mean value for the block width and ring radius which as shown previously is a valid assumption to make. This aspect of the calculation depends on the uncertainty in the digital acquisition system and the LVDT. The individual contributions of these systems and the overall uncertainty is shown in Table 12 Overall uncertainty is calculated by taking the root sum of squares of each individual contribution which is then multiplied by a factor of $\sqrt{2}$ because, similar to the mass loss measurement, this measurement is calculated from the difference between the initial and final displacements of the LVDT. Fortunately, the manufacturers of the LVDT provided the uncertainty as part of their calibration certification and were the only company whose products are used in this tribometer to do so. Here we can see that the uncertainty is beginning to approach a level within an order of magnitude of the true value being measured, however any direct measurement change in length at these small scales is not trivial. Uncertainty in this measurement that would be caused by the eccentricity of the ring has been omitted because the implementation of an encoder lets the height of the LVDT be sampled at exactly the same position for every cycle.

Source	Typical Wear Scar Depth (mm)	Uncertainty (mm)	% of Uncertainty	% of Mean
LVDT Calibration Uncertainty	1.00	0.0115	1.88%	1.19%
LVDT Linearity	1.00	0.0857	98.07%	8.57%
AD Conversion Resolution	1.00	0.0007666	0.01%	0.01%
AD Conversion Noise	1.00	0.00177	0.04%	0.18%
Wear Scar Depth		**0.0866**		**8.66%**

Table 12: Wear scar depth uncertainty

Combining These Components

Finally, it is necessary to combine these components of the uncertainty of the block's volume loss into the total value. Using equations (5) through (10), it is possible to calculate the overall uncertainty of the volume loss which is shown in Table 13. Again, this value is unacceptable. The main contribution to this high uncertainty is the accuracy of LVDT. Therefore, to lower uncertainty it may be easier to use another technique to measure block volume loss such as white light interferometry to measure and calculate the volume of the wear scar using a technique similar to that described by Colbert et all (2011).[27] An even better method would be to measure the mass loss of the block, similar to the ring. However, if more volume is worn away during the test, this uncertainty could reach an acceptable value.

Source	Typical Value (mm)	Uncertainty (mm)	% of Uncertainty	% of Mean
Ring Radius	12.72	0.0284	15.0%	0.22%
Wear Scar Depth	1.00	0.0866	69.7%	8.66%
Block Width	6.31	0.0287	15.3%	0.45%
Block Volume Loss	**41.94mm³**	**21.09mm³**		**52.22%**

Table 13: Block volume loss uncertainty

Sliding Distance

Another value needed to quantify the uncertainty in wear rate is sliding distance. Sliding distance depends on the number of cycles run, the stroke of each cycle, and the circumference of the ring used in the test. Some error arises here from limitations in the control of the motor.

During initial testing, there was some variability in the number of cycles the machine would use to conduct a test, but this has since been remedied through improved coding and thus contributes no uncertainty. However, the motor controller only tracks the rotation of the motor using 8-bits of precision which works out to a resolution of 1.4° and will therefore have trouble resolving a difference of, on average, 2.6°. The error caused by this limitation is able to be tracked due to the implementation of an external encoder with an angular resolution of .088°. This higher resolution position data from the external encoder

can then be used to increase the accuracy of the wear data through more exact knowledge of total sliding distance.

Four different tests were examined to evaluate the variation in the stroke of the tribometer which resulted in the following data in Table 15. Each test consists of between 3355 to 5721 complete cycles and so the average stroke over the length of the test is used. It is evident that not only is there some uncertainty in the actual length of each stroke, but also that there is a bias error which results in the stroke being consistently shorter than programmed. Not accounting for this bias error, the results of this aspect of the uncertainty analysis are as follows in Table 14. It shows that the sliding distance has low uncertainty and that the current method used for measuring this distance is valid. The derivation of the uncertainty of the total sliding distance during a test follows these equations:

$$u_c(d) = c\sqrt{\left(\frac{\partial d}{\partial s}\right)^2 u^2(s) + \left(\frac{\partial d}{\partial r}\right)^2 u^2(r)} \tag{11}$$

$$\frac{\partial d}{\partial s} = \frac{\pi r n}{180} \tag{12}$$

$$\frac{\partial d}{\partial r} = \frac{\pi s n}{180} \tag{13}$$

Test #	Commanded Stroke (°)	Mean Measured Stroke (°)	Standard Deviation (°)	% of Mean
1	360	357.24	0.18	0.05%
2	360	357.64	0.11	0.03%
3	360	357.43	0.18	0.05%
4	360	357.15	0.12	0.03%
Mean		357.37	0.15	0.04%

Table 15: Experimental data examining differences in commanded stroke vs actual stroke

Source	Typical Value	Uncertainty	% of Uncertainty	% of Mean
# of Cycles	5000	0	0.0%	0.0%
Actual Stroke	357.6°	0.10°	0.68%	0.03%
Resolution of Encoder	0.088°	0.78°	98.31%	0.22%
Stroke Uncertainty	357.6°	0.79°	49.26%	0.221%
Ring Radius Uncertainty	12.72mm	0.0285mm	50.74%	0.224%
Sliding Distance	**396.95m**	**1.24m**		**0.31%**

Table 14: Sliding distance uncertainty

Normal force

The final component necessary to calculate wear rate is the normal force. This value is also used in the calculation of friction coefficient. As previously discussed, due to the use of reciprocating motion, errors that would arise in the measurement of force are eliminated and thus not included in this analysis. Uncertainty now arises in this measurement from the load cell and the DAQ system. Noise in the system was calculated from the data recorded in the earlier described experiment regarding noise in the LVDT signal except using the data recorded from the F_Z channel of the load cell. Thus, the uncertainty is shown in Table 16, calculated from the root sum of squares of its components, and is sufficiently low to trust the measurement of normal force at less than one percent of the value specified in the example experiment.

Source	Typical Value (N)	Uncertainty (N)	% of Uncertainty	% of Mean
Load Cell Linearity	500	4.44	99.24%	0.89%
AD Conversion Resolution	500	0.39	0.76%	0.08%
AD Conversion Noise	500	0.01	0.04%	0.00%
Normal Force		**4.46**		**0.89%**

Table 16: Normal force uncertainty

Friction force

The final measurement made with the tribometer is that of friction force. This is required to calculate the friction coefficient of the material system. The sources of uncertainty in this measurement are the same as that for the normal force along with the overall calculation, but different values result due to differences in the load cell sensitivity in the F_z and F_x axes, the different signal path and amplification,

Source	Typical Value (N)	Uncertainty (N)	% of Uncertainty	% of Mean
Load Cell Linearity	100	3.19	96.33%	3.19%
AD Conversion Resolution	100	0.62	3.67%	0.31%
AD Conversion Noise	100	0.003	0.00%	0.00%
Friction Force		**3.25**		**3.25%**

Table 17: Friction force uncertainty

and the typical values used for each. Table 17 shows the uncertainty in the measurement of friction force. Similar to the measurement of normal force, the measurement of friction force also has sufficiently low uncertainty to trust this measurement, albeit as a higher percentage of the mean value from the prototype experiment. This is due mainly to the mean value of friction force being lower than the normal force.

Overall Uncertainty

With all the groundwork, out of the way, it is now possible to calculate the total uncertainty of the measurements made by the tribometer. Starting with the equation for wear rate, the derivation of the uncertainty in the wear rate of the ring is as follows:

$$K_{ring} = \frac{V_{L,ring}}{F_N d} \tag{14}$$

$$u_c(K_{ring}) = c\sqrt{\left(\frac{\partial K_{ring}}{\partial F_N}\right)^2 u^2(F_N) + \left(\frac{\partial K_{ring}}{\partial d}\right)^2 u^2(d) + \left(\frac{\partial K_{ring}}{\partial V_{L,ring}}\right)^2 u^2(V_{L,ring})} \tag{15}$$

$$\frac{\partial K_{ring}}{\partial F_N} = -\frac{V_{L,ring}}{dF_N^2} \tag{16}$$

$$\frac{\partial K_{ring}}{\partial d} = -\frac{V_{L,ring}}{F_N d^2} \tag{17}$$

$$\frac{\partial K_{ring}}{\partial V_{L,ring}} = \frac{1}{F_N d} \tag{18}$$

The calculation of the uncertainty of the wear rate of the ring follows a similar path and also starts with the equation for wear rate:

$$K_{block} = \frac{V_{L,block}}{F_N d} \tag{19}$$

$$u_c(K_{block}) = c\sqrt{\left(\frac{\partial K_{block}}{\partial F_N}\right)^2 u^2(F_N) + \left(\frac{\partial K_{block}}{\partial d}\right)^2 u^2(d) + \left(\frac{\partial K_{block}}{\partial V_{L,block}}\right)^2 u^2\left(V_{L,block}\right)} \tag{20}$$

$$\frac{\partial K_{block}}{\partial F_N} = -\frac{V_{L,block}}{d F_N^2} \tag{21}$$

$$\frac{\partial K_{block}}{\partial d} = -\frac{V_{L,block}}{F_N d^2} \tag{22}$$

$$\frac{\partial K_{block}}{\partial V_{L,block}} = \frac{1}{F_N d} \tag{23}$$

Finally, the calculation for the uncertainty of the friction coefficient measurement begins with the equation for friction coefficient:

$$\mu = \frac{F_f}{F_N} \tag{24}$$

$$u_c(\mu) = c\sqrt{\left(\frac{\partial \mu}{\partial F_N}\right)^2 u^2(F_N) + \left(\frac{\partial \mu}{\partial F_f}\right)^2 u^2\left(F_f\right)} \tag{25}$$

$$\frac{\partial \mu}{\partial F_N} = -\frac{F_f}{F_N^2} \tag{26}$$

$$\frac{\partial \mu}{\partial F_f} = \frac{1}{F_N} \tag{27}$$

Solving these equations using the experimental conditions and typical values of the prototype experiment. gives the following results shown in Table 18. From this we can tell that measuring the wear

Measurement	Reported Value	Uncertainty	% of Reported Value
Wear Rate (Block)	2.11×10^{-4} mm³/Nm	1.12×10^{-4} mm³/Nm	52.23%
Wear Rate (Ring)	6.40×10^{-5} mm³/Nm	6.06×10^{-7} mm³/Nm	0.95 %
Friction Coefficient	0.20	6.73×10^{-3}	3.37%

Table 18: Wear rate and friction coefficient total uncertainties

rate the block in this experiment is unfeasible, while measurements of the ring wear rate are valid. Also, the friction coefficient value reported by the tribometer is adequately robust for the experimental method

described at the beginning of the uncertainty analysis. Thankfully, for this experiment, which is discussed later in this paper as a case study, wear rates were not of interest while friction coefficient was.

Uncertainty Budget

An uncertainty analysis does not only quantify the level to which a device's measurements can be trusted. By knowing each individual component's uncertainty along with the total uncertainty an uncertainty budget can be created. This budget shows how much each individual component contributes to the overall uncertainty and was inspired by a more limited uncertainty budget calculated by Schmitz et all (2004). [28] This information can then be used to decide where the machine most needs improvement to reduce overall uncertainty. Tables Table 19, Table 21, and Table 20 shows these uncertainty budgets for each measurement. From this analysis it is evident that for the block wear rate by far the largest contribution to uncertainty in wear rate is the methods used to measure the volume loss of the sample. As discussed previously, a more accurate method to measure this volume loss would be to measure mass loss of the block in addition to the ring. Uncertainty in the ring wear rate is due to the variation in the normal force which has been the subject of intense effort to minimize. Further efforts to minimize this would involve replacing the pneumatic thruster with a lower inertia component such as a flexure based system. This analysis also shows that for friction coefficient analysis the limiting factor is the inherent performance of the load cell. This could possibly be improved through some clever characterization of the nonlinearity of the load cell to correct that error, but it is more likely that a higher performing load cell would be necessary.

Uncertainty Budget	% of Level 1	% of Level 2	% of Level 3
Wear Rate (Block)	100.00%		
Volume Loss	99.97%	100.00%	
Ring Radius Uncertainty	0.18%	0.18%	100.00%
Caliper Accuracy	0.03%	0.03%	16.51%
Caliper Resolution	0.12%	0.12%	66.06%
Caliper Repeatability	0.03%	0.03%	16.51%
Ring Radius Actual Variation	0.00%	0.00%	0.92%
Wear Scar Depth Uncertainty	99.78%	99.81%	100.00%
LVDT Calibration Uncertainty	1.88%	1.88%	1.88%
LVDT Linearity	97.85%	98.88%	98.07%
AD Conversion Resolution	0.01%	0.01%	0.01%
AD Conversion Noise	0.04%	0.04%	0.04%
Block Width Uncertainty	0.01%	0.01%	100.00%
Caliper Resolution	0.00%	0.00%	16.21%
Caliper Accuracy	0.00%	0.00%	64.83%
Caliper Repeatability	0.00%	0.00%	16.21%
Block Width Actual Variation	0.00%	0.00%	2.76%
Sliding Distance	0.00%	100.00%	
Ring Radius Uncertainty	0.00%	50.74%	100.00%
Caliper Accuracy	0.00%	8.38%	16.51%
Caliper Resolution	0.00%	33.52%	66.06%
Caliper Repeatability	0.00%	8.38%	16.51%
Ring Radius Actual Variation	0.00%	0.46%	0.92%
Stroke Uncertainty	0.00%	49.26%	100.00%
Actual Stroke Variation	0.00%	0.83%	1.69%
Resolution of Encoder	0.00%	48.43%	98.31%
Normal Force	0.03%	100.00%	
Load Cell Linearity	0.03%	96.33%	
AD Conversion Resolution	0.00%	3.67%	
AD Conversion Noise	0.00%	0.00%	

Table 19: Block wear rate uncertainty budget

Uncertainty Source	% of Level 1	% of Level 2	% of Level 3
Wear Rate (Ring)	**100.00%**		
Mass Loss	1.07%	100.00%	
Scale Repeatability	0.24%	22.10%	
Scale Resolution	0.06%	5.53%	
Typical Use	0.77%	72.37%	
Sliding Distance	10.88%	100.00%	
Ring Radius Uncertainty	5.52%	50.74%	100.00%
Caliper Accuracy	0.91%	8.38%	16.51%
Caliper Resolution	3.65%	33.52%	66.06%
Caliper Repeatability	0.91%	8.38%	16.51%
Ring Radius Actual Variation	0.05%	0.46%	0.92%
Stroke Uncertainty	5.36%	49.26%	100.00%
Actual Stroke Variation	0.09%	0.83%	1.69%
Resolution of Encoder	5.27%	48.43%	98.31%
Normal Force	88.06%	100.00%	
Load Cell Linearity	84.82%	96.33%	
AD Conversion Resolution	3.24%	3.67%	
AD Conversion Noise	0.00%	0.00%	

Table 21: Ring wear rate uncertainty budget

Uncertainty Source	% of Level 1	% of Level 2
Friction Coefficient	**100.00%**	
Normal Force	7.02%	100.00%
Load Cell Linearity	6.76%	96.33%
AD Conversion Resolution	0.26%	3.67%
AD Conversion Noise	0.00%	0.00%
Friction Force	92.98%	100.00%
Load Cell Linearity	89.56%	96.33%
AD Conversion Resolution	3.42%	3.67%
AD Conversion Noise	0.00%	0.00%

Table 20: Friction coefficient uncertainty budget

Sensitivity to purposeful errors

We were also interested in the tribometer's real world response to errors. This was tested by introducing various purposeful and quantifiable errors in the setup of the machine. All of these experiments were set up to use the block on ring configuration of the tribometer.

The first of these errors tested was that of ring eccentricity. To test this, special rings were made that had a purposeful offset between the taper and outside running surface, shown in Figure 24: Part

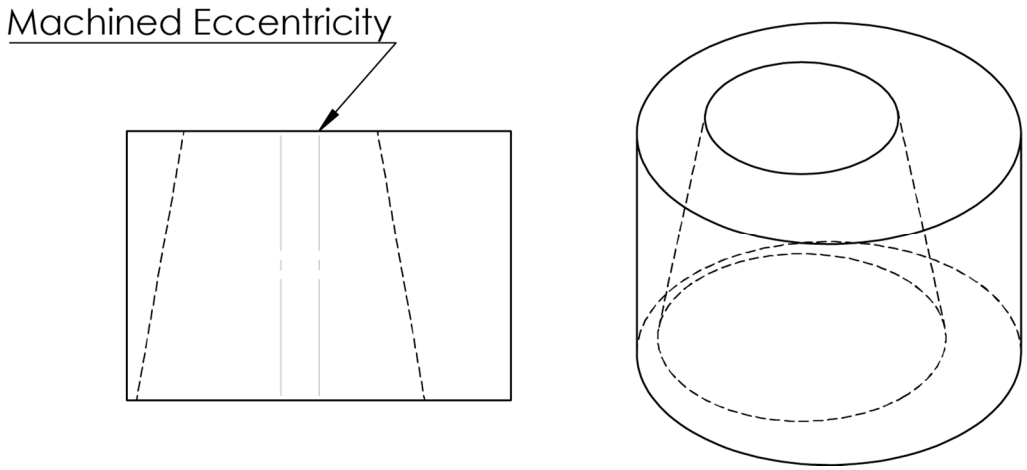

Figure 24: Part diagram of purposefully eccentric ring

diagram of purposefully eccentric ring. Two sets of four rings were made in this fashion, one set with an eccentricity of .001" and the other set with .002" eccentricity. We then mounted these rings on the tribometer's spindle and measured the runout of each. We found that the eccentricity of the rings varied from .0009" to .0043", much greater than the range of eccentricity than could be provided by the purposeful eccentricity machined in the ring. This is attributed to the misalignment stack up between the collet and spindle, spindle and taper, and taper and outer ring surface. Regardless, this allowed us to test a wider range of eccentricities than initially planned. After measuring the

Parameter	Value
Normal Force (N)	500
Speed (rev/s)	2
Stroke (°)	360
# of Cycles	100
Lubricant	WD40 MUP

Table 22: Experimental parameters

eccentricity of the rings we conducted a 100 cycle reciprocating block on ring test using the test parameters in Table 22: Experimental parameters.

The raw data recorded from the experiment allowed us to see the effect of increased eccentricity on the variation of ring rotational velocity, the normal force, and the friction force. The results of these data analyses are displayed in Tables Table 24, Table 25, Table 23. These results show that most of these attributes of the tribometer are relatively unaffected by the increased eccentricity with the exception of normal force variation. It makes sense that normal force varies more with increased ring eccentricity as the ring will is pressed against the combined mass of the thruster and load cell and this eccentricity will vary the displacement of the load cell, thus varying the force it measures. These conclusions are additionally evident in the following series of graphs, Figure 25: Effect of ring eccentricity on normal force variation and Figure 26. All measured attributes seem relatively unaffected by the increased eccentricity except the normal force standard deviation. A simple way to quantify this difference is to compare the fit of the trend lines on each data set. The fit of the trend line for the standard deviation of the normal force is four times better than that of the data set with the next best fitting line. Furthermore, the lack of variation in the friction force measurement shows that we have good isolation between axes on the load cell. If our tribometer was set up so the load cell was tilted or the sample/countersample interface produced forces at an angle to the load cell, then this would be evident in these tests.

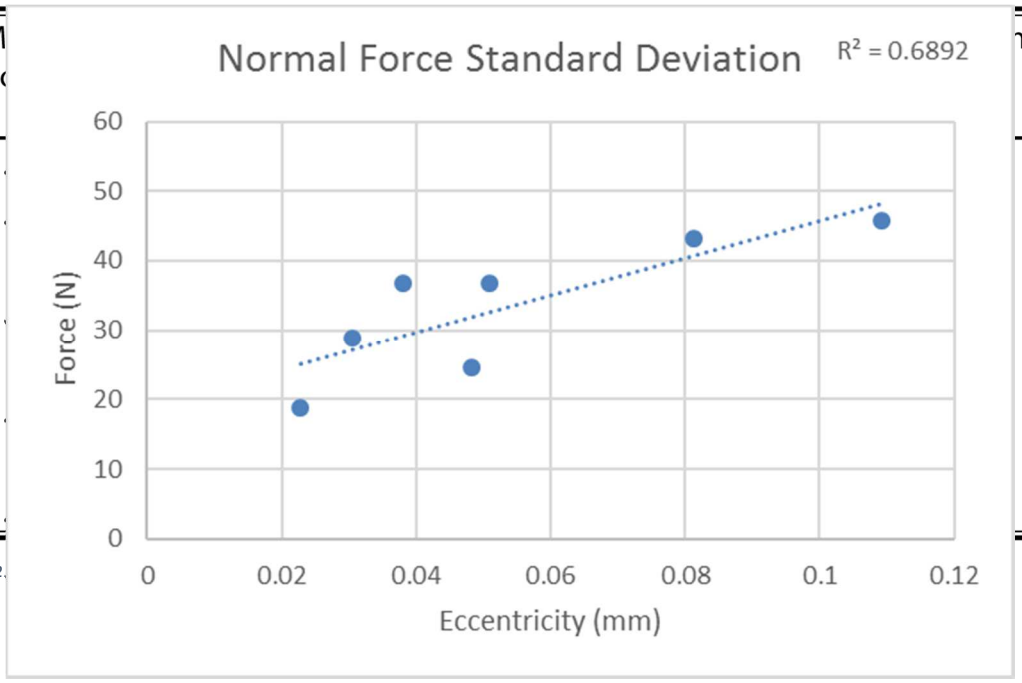

Figure 25: Effect of ring eccentricity on normal force variation

Measured Eccentricity (mm)	F_f Mean (N)	F_f Standard Deviation (N)	% of Mean
.02286	55.7	7.8	14.2%
.03048	55.6	3.5	6.3%
.0381	54.5	5.6	10.3%
.04826	50.6	9.8	19.5%
.0508	55.4	4.6	8.3%
.08128	49.0	8.3	17.0%
.1016	48.1	9.8	20.4%
.10922	58.3	6.8	11.7%

Table 23: Effect of ring eccentricity on friction force variation

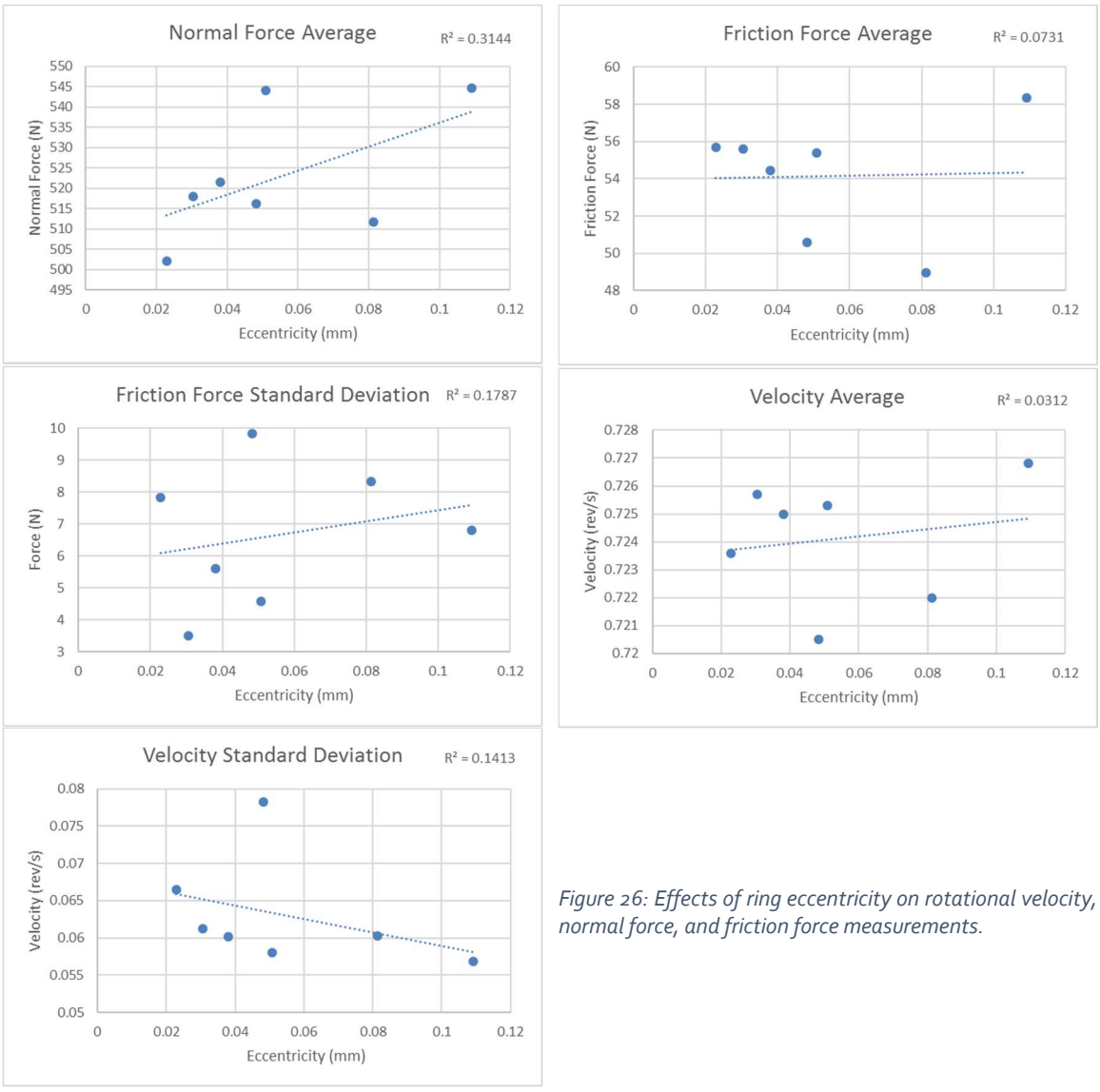

Figure 26: Effects of ring eccentricity on rotational velocity, normal force, and friction force measurements.

More in depth analysis of the variation in normal force compared to the eccentricity is provided in Figure 27. The normal force data from each cycle was fit to a sine curve and then had its amplitude extracted. The amplitude from every cycle in each experiment was then averaged and used to create a new

sine

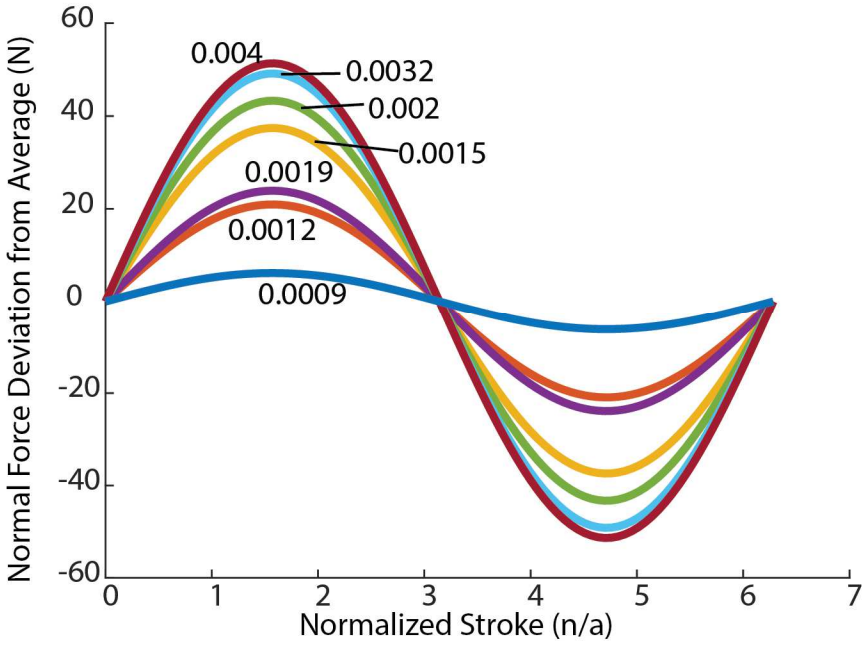

Figure 27: Averaged normal force variation across stroke for each eccentricity

function representing the average amplitude in the normal force variation for each eccentricity. These were then overlaid on one another which resulted in this figure. There is almost a uniform progression from lowest eccentricity and lowest normal force variation to the highest eccentricity and the highest normal force variation.

Measurement	Reported Value	Uncertainty	% of Reported Value
Wear Rate (Block)	2.11×10^{-4} mm³/Nm	1.12×10^{-4} mm³/Nm	52.23%
Wear Rate (Ring)	6.40×10^{-5} mm³/Nm	6.06×10^{-7} mm³/Nm	0.95%
Friction Coefficient	0.20	6.73×10^{-3}	3.37%

Table 26: Effect of added ring eccentricity on uncertainties

This data was the incorporated into the uncertainty analysis. For brevity's sake, only the final results have been included. The eccentricity of the ring added an 18N source of uncertainty to the

calculations regarding the total uncertainty of the normal force measurements. This result of this is shown in Table 26: Effect of added ring eccentricity:

Obviously, total uncertainty increases for all three measurements. However, this increase is nominal for the wear rate measurements which is a good sign; even if the ring exhibits eccentricity exceeding that of the ASTM standard these measurements remain similarly reliable. On the other hand, uncertainty in the friction coefficient measurement increases by about 50%. Fortunately, it remains low compared to the values typically measured on this machine, but this would become an issue trying to measure material systems that exhibit ultra-low friction.

Experiments informed by Uncertainty

Now that the uncertainty has been calculated for a single set of experimental parameters it is possible to adapt it to an extended parameter set. This has been calculated for the method of calculating wear rate from mass loss. This method was applied solely to the ring in the previous uncertainty analysis, but it will be valid for any wear rate calculated from mass loss with this equipment. In order to calculate the uncertainty across a wide range of experiments it is first desirable to reduce the number of free variables in the experiment. Whereas the previous uncertainty depended on normal force, number of cycles/sliding distance, volume loss, and wear rate; this analysis only requires a value for the material's wear rate and a combined F_nN factor. This factor is the normal force multiplied by the number of cycles in an experiment. This factor can then be split up into discrete numbers for normal force and cycles which are each represented by a single line in the graph. First it will be easiest to consider a graph which only displays one F_nN factor, shown in Figure 29. Each line represents a single combination of normal force and cycles number across the range of normal force values typical to this tribometer.

Several of these graphs can then be combined to paint a complete picture of the tribometer's uncertainty across a wide range of experimental parameters as is done in Figure 28. Finally, these graphs can have lines of constant error overlaid which can then be used to understand the necessary experimental parameters to design an experiment which will measure the wear rate of a material at a desired level of uncertainty. This graph is shown in Figure 30.

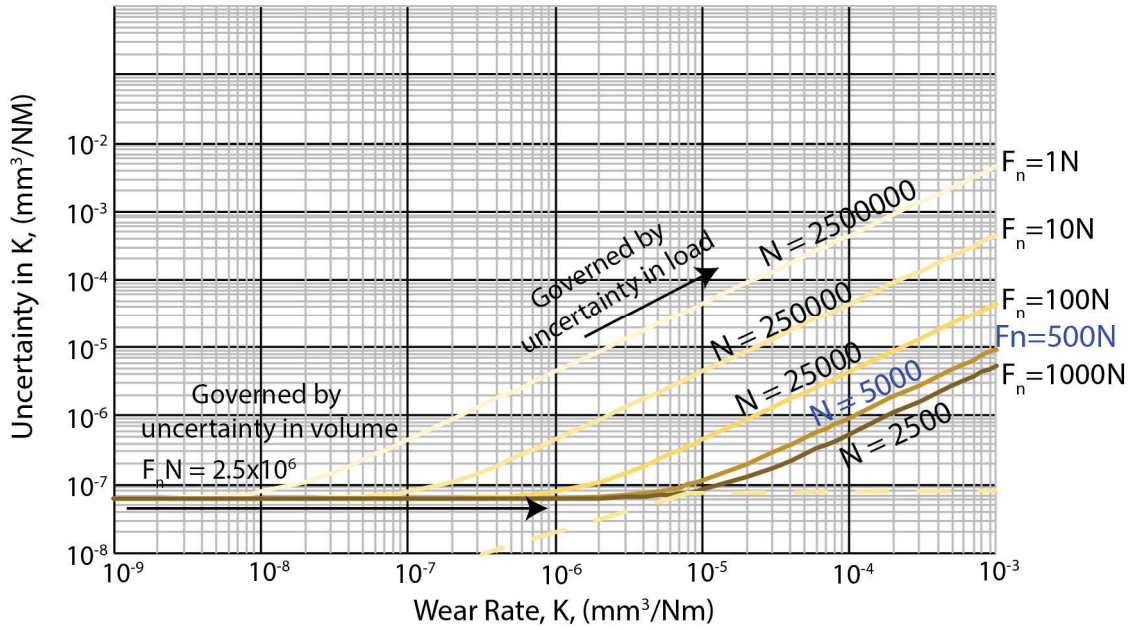

Figure 29: Uncertainty vs Wear Rate for FN = 2,500,000

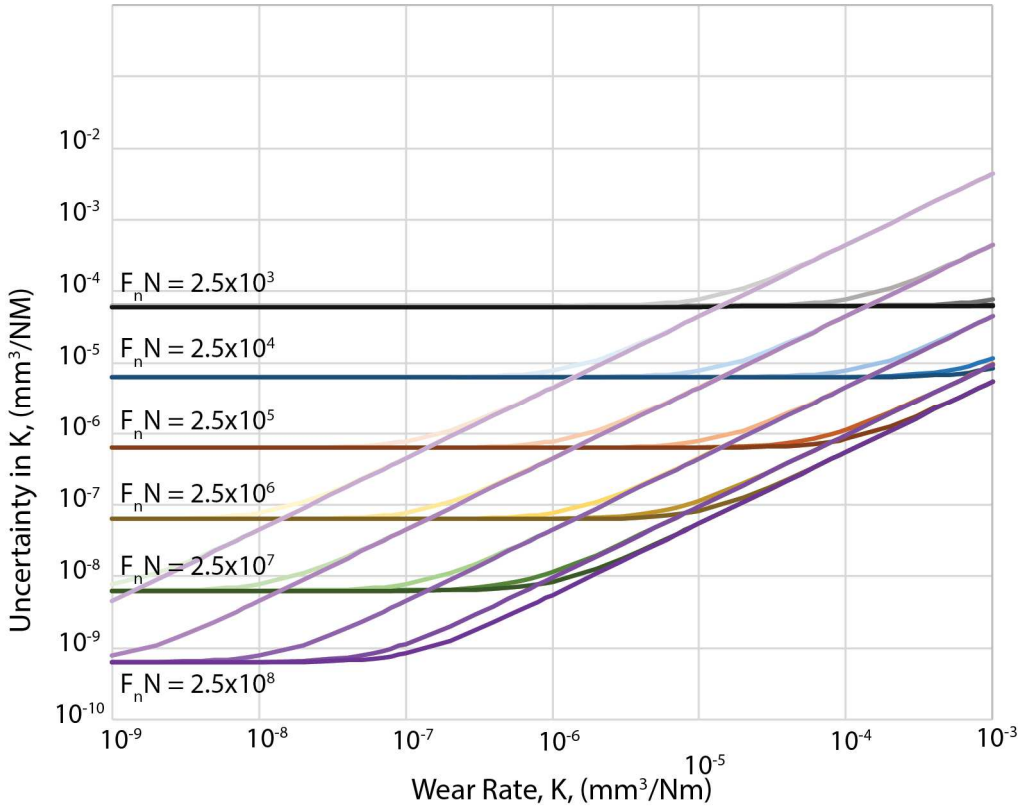

Figure 28: Uncertainty vs Wear Rate across multiple FN values

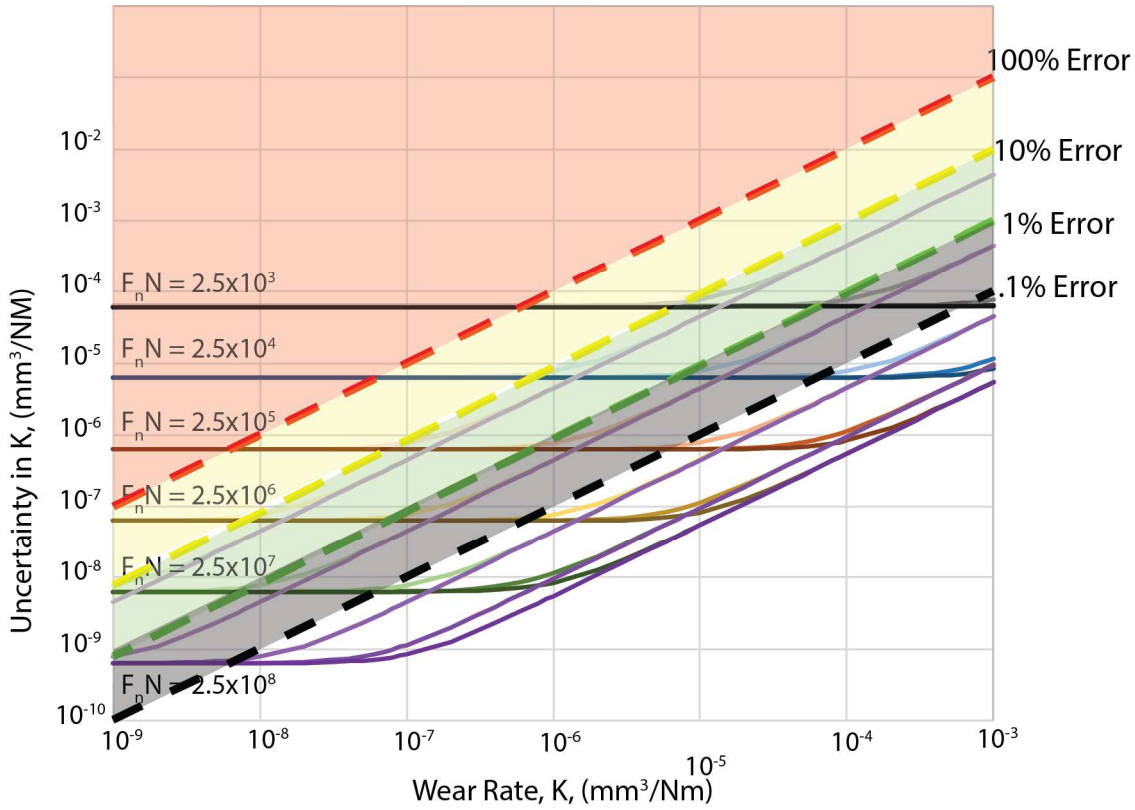

Figure 30: Experimental parameter space with lines of constant error

Case Study: Block on Ring testing using WD40 as a lubricant

The primary funding source for the multifunctional tribometer came from the WD40 corporation and as such it has been used for testing of their products. One such test focused on the lubricating properties of various formulations of WD40 in the block on ring configuration using a reciprocating test; the test parameters are listed in Table 27: Case study: experimental parameters for round one of WD40 testing. These initial rounds of testing were run until the instantaneous friction coefficient reached a value of .3 on twenty separate measurements. The machine then stopped reciprocating and recorded the number of cycles needed to reach this friction value. This ending condition was chosen as it roughly corresponded to the development of squeaking from the reciprocating contact. We surmised that at this point most consumers would reapply WD40 to quiet the squeaking so this was a realistic analogue to the real-world point when consumers would consider the WD40 worn away. The decision to make this threshold activate twenty times before stopping the test was to ensure that the test would not stop prematurely from a transient increase in friction due to the buildup of wear debris. These stop conditions can be visualized clearly in Figure 32: Example evolution of friction coefficient over the duration of a typical test. which displays the friction coefficient during several individual cycles from the first until the final cycle.

Parameter	Value
Normal Load (N)	500
Contact Pressure (MPa)	474
Angular Velocity (rev/s)	2
Stroke (°)	360
Friction Coefficient Threshold (instantaneous)	0.3

Table 27: Case study: experimental parameters for round one of WD40 testing

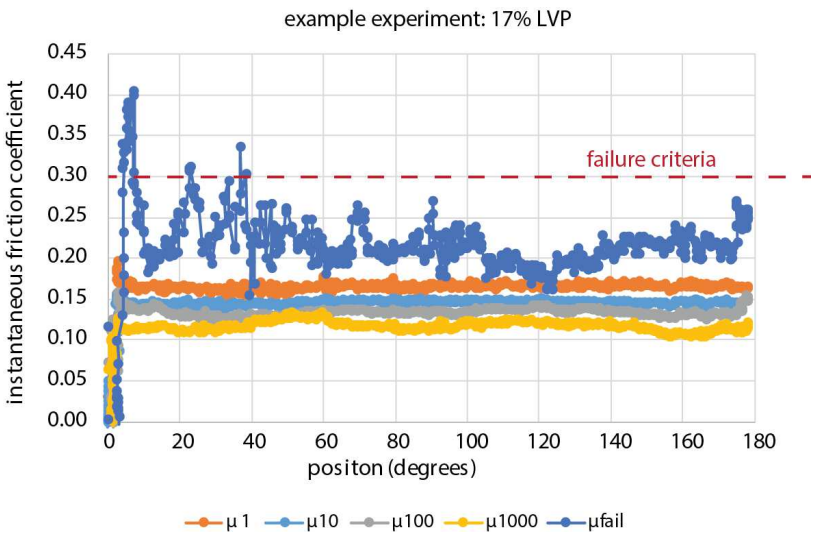

Figure 32: Example evolution of friction coefficient over the duration of a typical test.

The results from this first round of experiments is shown in the Figure 31. This shows how many cycles it took each test of each formulation to reach this threshold value for friction coefficient. No clear trends emerged to us from this data at first, but upon review of the operators' notes for each experiment some samples ended the test covered in an orange film, shown in Figure 34. Once these tests are singled out in the data it became apparent that these samples covered with the orange film remained low friction longer than tests which did not end with this film visible, shown in Figure 33. This led to a second round of experiments which aimed to control additional variables of the first experiment to hopefully draw out differences in the different formulations of WD40 and delve into what circumstances result in the creation of this orange film.

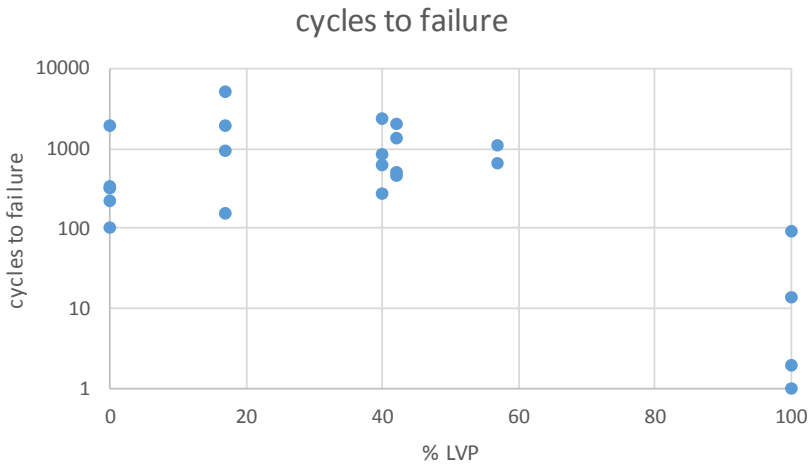

Figure 31: Round one experimental results

Figure 34: Left: ring after testing displaying orange film, Center: ring before testing, Right: ring after testing without orange film

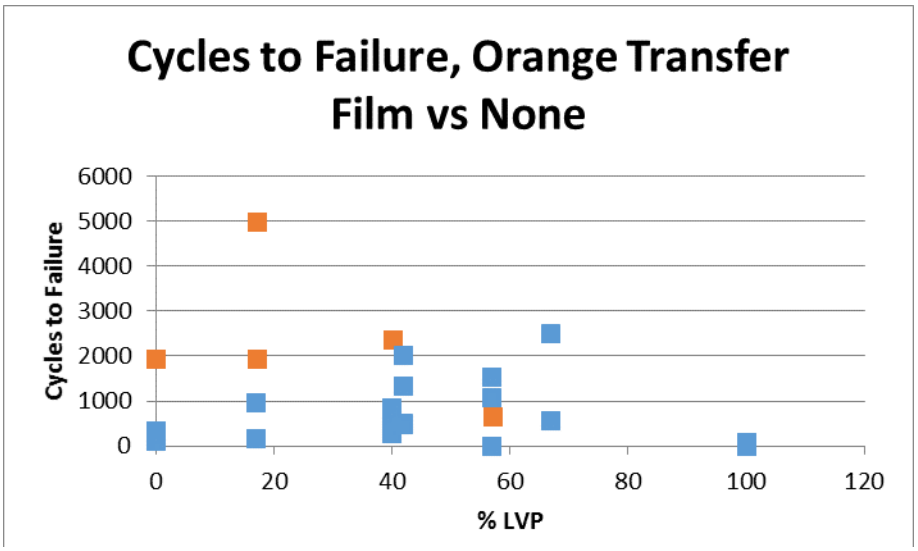

Figure 33: Round one test results, tests with orange films highlighted

To achieve these new goals several improvements were made the experimental setup. A calibrated pipet was used to dispense 10µL of WD40 onto the block for each run of the experiment. Now specifically thirty seconds would elapse between application of WD40 and the start of test motion to help control how much solvent would evaporate from the WD40 before the start of each test. New blocks were manufactured from machine key stock which resulted in much tighter tolerances. The end condition for the test was also altered. Now tests would run until the average friction throughout a cycle exceeded .25. To allow comparison to the first round of testing the tribometer also records the cycle when the instantaneous friction coefficient exceeds a value of .3 for the twentieth time. Testers would also note the

room's humidity at the time of the test as this affects the formation of many tribofilms. [29] The overall theme of these test method changes was to increase the number of variables controlled by the experiment to hopefully lower the large variability in data typically seen in tribology.

Additionally, an in-situ camera set up was to track the formation and destruction of the orange film. The camera is mounted on the tribometer using a 3D printed mount and controlled directly from MATLab along with the rest of the tribometer coding. Exposure and focus of the camera are locked so the color and brightness of separate tests can be directly compared. Additionally, the firing of the camera's shutter is coordinated through MATLab to take place at the same point in each cycle which allows for time lapse videos of the entire test to be created.

This second experiment produced more interesting results than the first as clear differences between the different WD40 formulations appeared. Using the in-situ camera system we were able to see that every experiment that was filmed displayed the orange transfer film. This point was missed on the previous round of experiments because the original ending condition of the instantaneous friction coefficient surpassing .3 was significantly more varied between tests than the new ending condition using the average cycle friction.

When comparing the cycles to failure and cycles to the instantaneous friction peak between different formulations a trend arises which correlates higher cycle counts to higher percentages of LVP in

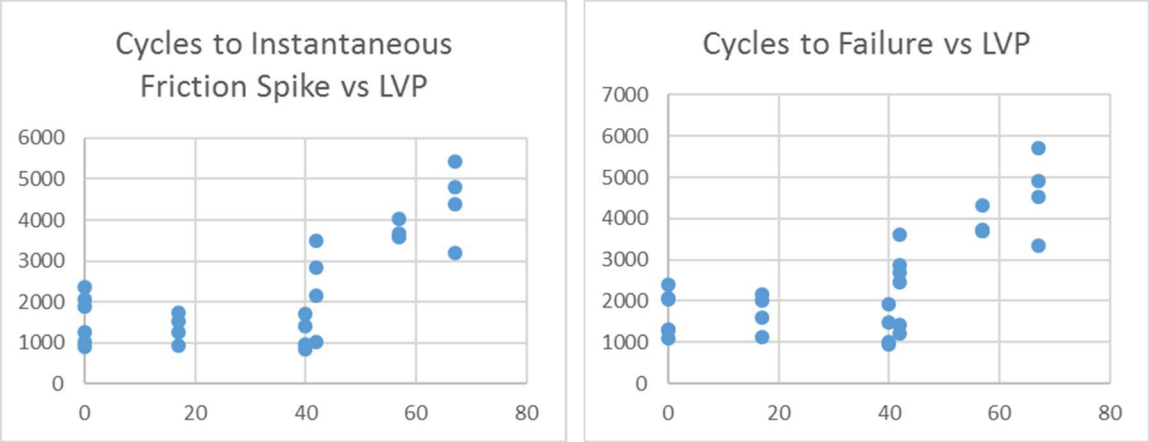

Figure 35: Results from second round of experiments

the mixtures, visible in Figure 35. Furthermore, the plots of these two values appear to be linearly offset from one another. This led to Figure 36, which shows the number of cycles elapsed between the instantaneous friction coefficient trigger and the end of the test. This offset does not appear to vary between different WD40 formulations.

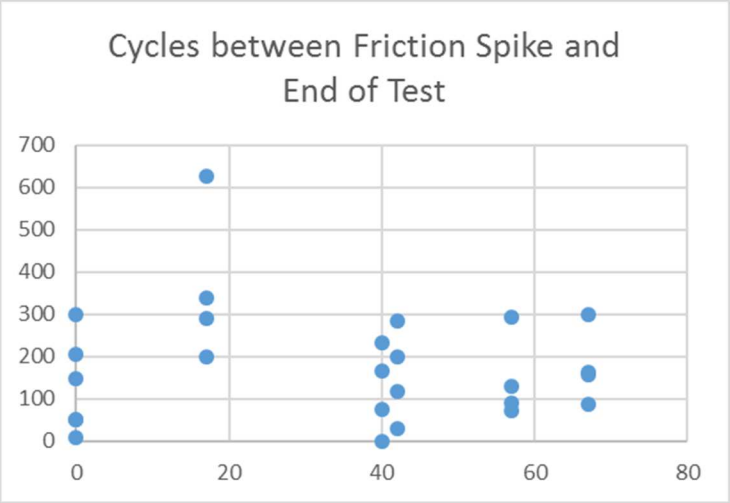

Figure 36: Cycles elapsed between onset of squeaking and end of test

This has an important implication in the use case of WD40, as failure of the lubricating film can now be predicted. The instantaneous trigger value was originally chosen as the end point of testing because the tribometer would begin squeaking. This round of experiments shows that almost universally the lubricating film provided by WD40 will fail soon after squeaking occurs at the material interface. While this may seem obvious, there was no concrete reason to assume that this squeaking would soon lead to failure of the lubricating film. This knowledge can allow users of the product to use squeaking as a sign to apply more WD40 instead of reapplying on a set time schedule which will lead to more economical and efficient use of WD40.

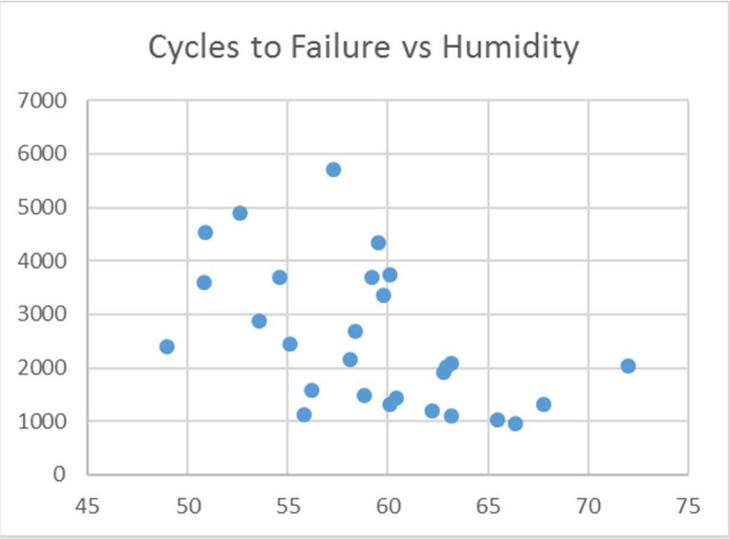

Figure 37: Cycles to failure vs humidity

Finally, as shown in Figure 37 it is somewhat unclear whether humidity influences the lubricating properties of WD40. The data recovered seems almost bimodal, with a change in behavior around

60% relative humidity. However, due to the highly variable nature of tribological testing and the fact that tests were only conducted across a range of 30% relative humidity more testing is needed to begin to draw any conclusions on this matter.

Future Work

Stroke Bias Error

The stroke of the rotation throughout each test displayed a bias error. The actual stroke would on average be 2.4° shorter than the commanded stroke of 360°. Further testing can be undertaken to try to identify if this bias error is constant across different commanded stroke values. Then a model can be created of this error as a function of the commanded stroke and implemented in the control code of the tribometer to compensate for this. Beyond this, the current motor controller has the capability to use the moment of inertia of the motor to inform its control of the motor. If this error is deemed desirable to reduce these avenues should be investigated first. If adjusting these properties does not provide a satisfactory reduction of error, then it is likely an improvement can only be realized through implementing a new motor controller.

Cosine Error

If the uncertainty analysis included here is found to be not representative of the tribometer's true accuracy throughout normal testing further sources of uncertainty can be explored. One such source is cosine error. Cosine error would be present in this tribometer is the error caused by misalignment between the normal and friction force vectors and the axes of the load cells. Through utilizing reciprocating motion along with careful construction of the machine including the use of alignment edges this error should be minimized beyond importance. However, it is always better to know absolutely and therefore this would be a valid line of investigation.

If there is found to be a higher than desired cosine error remedies can be implemented. During reconfiguration of the tribometer a protocol can be developed to measure the cosine error during reassembly and adjustments to the alignment of components can be made on the fly. Additionally, as the load cell measures force in the X, Y, and Z axes, friction force can be calculated from the sum of the X and Y forces to more accurately measure the friction force vector. If these improvements are not satisfactory, then sample mountings can be redesigned or remanufactured with more care and skill than was possessed by the operators at the initial construction of the tribometer.

Block Width/Block and Ring Misalignment

The initial method of producing blocks for testing resulted in significantly higher variation in the width of the blocks than the current commercial source of block blanks. Additionally, if the blocks are rotated in relation to the ring the apparent width of the line contact across the block will increase. This will change the contact pressure at the material interface and will also affect the accuracy of the calculated block volume loss. Therefore, it may be of interest to investigate the effect this change in contact length will have on the measurements made by the tribometer.

Higher Wear Rate Material System Testing

Having completed the uncertainty analysis of the block on ring configuration of the multifunctional tribometer it is apparent that the prototype experiment examined experiences wear rates below the detection threshold on the machine. Therefore, it would be of interest to conduct a test which can have its wear rates measured by the machine. A more suitable test would be a block on ring experiment using conformal contact between a polymer block and a metal ring. While this would still render the wear rate of the ring undetectable, it should provide an amount of material loss which would easily be measured through either the LVDT or mass loss methods examined in this paper.

Summary

In the interest of conducting friction and wear testing at a price point significantly lower than that of commercial tribometers while also including an increase in the versatility of the machine along with the amount of data available a multifunctional tribometer was designed and constructed. Once built, it was necessary to quantify the uncertainty in the measurements made by the tribometer to ensure its value and accuracy as a piece of scientific test equipment. Thus, an uncertainty calculation was conducted which resulted in the following conclusions. The current method used to calculate wear rate of ring samples is valid only for high wear rate materials such as unreinforced polymers. The wear rate measurement of the block sample is much more accurate and allows for the measurement of more wear resistant materials such as reinforced polymers and some metals. Friction coefficient measurements are valid for high to low friction systems, but then difficulties are encountered when entering the very low friction range.

Armed with this knowledge, a path to further reducing this uncertainty is clear. Improvements to the coding, construction, and recommendations for the upgrading of components are explained. This provides an economical and sensible path forward to improve the multifunctional tribometer.

Finally, a case study was carried out using the multifunctional tribometer. This case study is representative of1 the work typically done with the tribometer. The results of this experiment were further validated by the results of the uncertainty analysis. As testing only involved the measurement of friction coefficient and not wear rates the multifunctional tribometer's use was valid in this lubricated metal on metal material system.

Moving forward, the multifunctional tribometer's valid experimental space is now known. This allows for results from this machine to be trusted and to be disseminated amongst the scientific community.

References

[1] Jost, H.P., Lubrication (Tribology): Education and Research - A Report on the Present Position and Industry's Needs, Her Majesty's Stationery Office. (1966).

[2] Jost, H.P., Tribology - Origin and future, Wear 136, 1-17 (1990).

[3] D.L. Burris, W.G. Sawyer, Tribological Sensitivity of PTFE/Alumina Nanocomposites to a Range of Traditional Surface Finishes, Tribol. Trans. 48 (2005) 147–153. doi:10.1080/05698190590923842.

[4] E. Smazalová, Š. Houdková, M. Švantner, Tribological effects of discontinuous Block-on-Ring test, in: Met. 2014 - 23rd Int. Conf. Metall. Mater., 2014: pp. 1004–1010.

[5] R.J. Moffat, Describing the uncertainties in experimental results, Exp. Therm. Fluid Sci. 1 (1988) 3–17. doi:10.1016/0894-1777(88)90043-X.

[6] S. Bell, A Beginner's Guide to Uncertainty of Measurement Measurement Good Practice Guide, (n.d.).

[7] J.A. Williams, Wear and wear particles—some fundamentals, Tribol. Int. 38 (2005) 863–870. doi:10.1016/j.triboint.2005.03.007.

[8] T.L. Schmitz, J.E. Action, J.C. Ziegert, W.G. Sawyer, The Difficulty of Measuring Low Friction: Uncertainty Analysis for Friction Coefficient Measurements, J. Tribol. 127 (2005) 673. doi:10.1115/1.1843853.

[9] D.-H. Cho, J.-S. Kim, J. Jia, Y.-Z. Lee, Comparative analysis based on adiabatic shear instability for scuffing failure between unidirectional and reciprocating sliding motion, Wear. 297 (2012) 774–780. doi:10.1016/j.wear.2012.10.014.

[10] D.L. Burris, A.W.G. Sawyer, Addressing Practical Challenges of Low Friction Coefficient Measurements, (n.d.). doi:10.1007/s11249-009-9438-2.

[16] Ultramation, Four Shaft Linear Thrusters. http://www.ultramation.com/Catalog/cat4sweb.pdf.

[17] Parker Motion, MPP/MPJ Series Low & High lnertia Rotary Servo Motors. http://www.parkermotion.com/bbs/MPP/MPP_MPJ_Catalog_02_04_08.pdf

[18] Parker Motion, Compax3 Series Servo Drives & Controllers. http://www.parkermotion.com/literature/Compax3Brochure_Sept2010.pdf

[19] Gilman Precision, Gilman Spindles Catalog. http://www.gilmanprecision.com/wp-content/uploads/2016/10/Spindle-Catalog-10-7-16.pdf

[20] AMTI, MC3A-1000 Specifications. http://amti.biz/

[21] RDP Group, DCTH Series DC to DC LVDT Displacement Transducer. http://www.rdpe.com/us/dcth.pdf.

[22] National Instruments, NI 6321 - Device Specifications. http://www.ni.com/pdf/manuals/374461b.pdf

[11] Standard Test Method for Calibration and Operation of the Falex Block-on-Ring Friction and Wear Testing Machine 1, 94 (2011) 2009–2012. doi:10.1520/D2714-94R09.5.2.

[12] Standard Test Method for Ranking Resistance of Materials to Sliding Wear Using, Wear. 5 (2010) 1–11. doi:10.1520/G0077-05R10.2.

[13] Standard Test Method for Ranking Resistance of Plastic Materials to Sliding Wear, Wear. 14 (2007) 1–7. doi:10.1520/G0137-97R09.2.

[14] Standard Test Method for Ranking Resistance of Plastics to Sliding Wear Using Block-on-Ring Wear Test — Cumulative Wear Method 1, Wear. 3 (2011) 1–9. doi:10.1520/G0176-03R09.2.

[15] Standard Test Method for Wear Rate and Coefficient of Friction of Materials in Self-Lubricated Rubbing Contact Using a Thrust Washer Testing Machine, ASTM Int. D 3702-9 (2004) 1–5. doi:10.1520/D3702-94R09.2.

[23] A. Damodaran, New York University, Statistical Distributions. http://people.stern.nyu.edu/adamodar/New_Home_Page/StatFile/statdistns.htm.

[24] MT XS205DU scale spec sheet. http://www.mt.com/dam/P5/labtec/Product_Brochures/XS/30208643_BR_en_XS_Balances_LR_07_2015.pdf

[25] Weisstein, Eric W. Circular Segment. MathWorld--A Wolfram Web Resource. http://mathworld.wolfram.com/CircularSegment.html

[26] ABSOLUTE Digimatic Caliper SERIES 500 — with Exclusive ABSOLUTE Encoder Technology. http://www.farnell.com/datasheets/92833.pdf

[27] R.S. Colbert, B.A. Krick, A.C. Dunn, J.R. Vail, N. Argibay, W.G. Sawyer, Uncertainty in pin-on-disk wear volume measurements using surface scanning techniques, Tribol. Lett. 42 (2011) 129–131. doi:10.1007/s11249-010-9744-8.

[28] T.L. Schmitz, J.E. Action, D.L. Burris, J.C. Ziegert, W.G. Sawyer, Wear-Rate Uncertainty Analysis, J. Tribol. 126 (2004) 802. doi:10.1115/1.1792675.

[29] J.F. Curry, N. Argibay, T. Babuska, B. Nation, A. Martini, N.C. Strandwitz, M.T. Dugger, B.A. Krick, Highly Oriented MoS2 Coatings: Tribology and Environmental Stability, Tribol. Lett. 64 (2016) 11. doi:10.1007/s11249-016-0745-0.

Vita

Michael Goldstein was born on November 23rd, 1992 to Jeffrey Goldstein and Lorraine Kolibas in Plainfield, NJ, USA. He received his Bachelor of Science in Mechanical Engineering from The George Washington University in Washington, DC in the spring of 2014. The following fall he began pursuing a Master of Science in Mechanical Engineering at Lehigh University intending to graduate in the fall of 2016.